Serine arginine-rich splicing factor (SRSF7) cooperates with the histone methyltransferase KMT5a to promote the type I interferon response via transcriptional activation of IRF7

Haley M. Scott[1], Mackenzie H. Smith[1], Aja K. Coleman[1], Summer L. Apostalo[1], Allison R. Wagner[1], Robert O. Watson[1], Kristin L. Patrick[1*#]

[1]Department of Microbial Pathogenesis and Immunology, Texas A&M Health, School of Medicine

*Corresponding author: kpatrick03@tamu.edu
#Lead contact
Phone: (979) 436-0354
Twitter: @The_PW_Lab

SUMMARY

Tight regulation of macrophage immune gene expression is required to fight infection without risking harmful inflammation. The contribution of RNA binding proteins (RBPs) to shaping the macrophage response to pathogens remains poorly understood. Transcriptomic analysis revealed that a member of the serine/arginine-rich (SR) family of mRNA processing factors, SRSF7, is required for optimal expression of a cohort of interferon stimulated genes (ISGs) in macrophages. Using genetic and biochemical assays, we discovered that in addition to its canonical role in regulating alternative splicing, SRSF7 drives transcription of interferon regulatory transcription factor 7 (IRF7) to promote antiviral immunity. At the *Irf7* promoter, SRSF7 maximizes STAT1 transcription factor binding and RNA polymerase II elongation via cooperation with the H4K20me1 histone methyltransferase KMT5a (SET8). These studies define an unorthodox role for an SR protein in activating transcription and reveal an unappreciated RNA binding protein-chromatin network that orchestrates macrophage antiviral gene expression.

62 **INTRODUCTION**

63 Macrophages (MΦ) are innate immune cells that serve as the body's first line of defense
64 against pathogens. They express a panoply of pattern recognition receptors that detect pathogen-
65 and damage-associated molecular patterns (PAMPs and DAMPs) and transmit these "danger
66 signals" to the nucleus though complex signal transduction cascades. Generally, these pathogen
67 sensing cascades terminate with phosphorylation and nuclear translocation of specialized im-
68 mune transcription factors (e.g. NFκB, IRF3, IRF7). Because innate immune transcription factors
69 exert control over hundreds of genes with massive inflammatory potential, their misregulation can
70 have dire consequences for a host: innate responses that are too weak enable pathogen survival
71 and replication, whereas responses that are too strong can trigger a cytokine storm, chronic in-
72 flammation, and autoimmunity. While the mechanisms through which innate immune transcription
73 factors are regulated post-translationally—via phosphorylation, dimerization, and nuclear translo-
74 cation—are well-established (Caamano and Hunter, 2002; Jefferies, 2019; Ning et al., 2011;
75 Smale, 2012), how cells control expression of these master regulators at the transcriptional and
76 post-transcriptional levels remains less well-understood.

77 A growing literature has built a strong case for RNA binding proteins (RBPs) in shaping
78 the transcriptomes of specialized cells like macrophages. SR (serine-arginine rich) proteins are a
79 15-member family of RBPs that are broadly defined as regulators of alternative splicing. By virtue
80 of distinct RNA recognition motifs, SRs bind to unique exonic splicing enhancers to help direct
81 the spliceosome to cis-splicing signals in target transcripts (Wagner and Frye, 2021). While best
82 known for their role in pre-mRNA splicing, SRs can participate in virtually any step of RNA pro-
83 cessing, from transcription all the way to translation (Jeong, 2017). These studies of SR function
84 have mostly been carried out in genetically tractable "model" cell lines (e.g. K562, HEK293T, and
85 HepG2), but we are beginning to appreciate specialized roles for SR proteins in immune cells.
86 SRSF1 is required for regulatory T cell homeostasis and function (Katsuyama and Moulton, 2021)
87 and several SR proteins have been implicated in T cell development via controlling alternative
88 splicing of CD45 (Lemaire et al., 1999; ten Dam et al., 2000; Wang et al., 2001). We recently
89 implicated SRSF6 in maintaining mitochondrial homeostasis and antiviral immunity in macro-
90 phages by controlling alternative splicing of the pro-apoptotic factor BAX (Wagner et al., 2022).

91 Intriguingly, differential phosphorylation of SR proteins has been reported in macrophages
92 infected with intracellular pathogens like the bacterium *Mycobacterium tuberculosis* (Budzik et al.,
93 2020) and the fungal pathogen *Cryptococcus neoformans* (Pandey et al., 2017). As phosphory-
94 lation of SR proteins regulates their localization and function (Misteli et al., 1998; Shin et al., 2004;
95 Zhong et al., 2009; Zhou and Fu, 2013), these macrophage phosphoproteomics studies suggest

96 that functionalization of SR proteins can occur downstream of pattern recognition receptor en-
97 gagement. We hypothesized that these SR proteins play privileged roles in tuning the macro-
98 phage response to pathogens. Indeed, we found that stable knockdown of several SR proteins in
99 RAW 264.7 macrophage-like cells (RAW MΦs) profoundly altered the transcriptome in resting and
100 activated macrophages (4h post-*Salmonella* Typhimurium infection) (Wagner et al., 2021). The
101 absence of one of these proteins, SRSF7, generated some particularly interesting phenotypes.
102 SRSF7 (formerly known as 9G8) is a canonical member of the SR protein family. It encodes an
103 RNA recognition motif (RRM) and an eponymic SR domain. It is the only SR family protein to also
104 encode a CCHC-type Zn knuckle domain, which is thought to contribute to its RNA-binding spec-
105 ificity (Cavaloc et al., 1999; Cavaloc et al., 1994; Wang et al., 2021)). To date, its function is best
106 studied in the context of controlling its own expression levels via poison cassette exon inclusion
107 (Konigs et al., 2020), in regulating mRNA export (Muller-McNicoll et al., 2016), and in alternative
108 splicing (Kadota et al., 2020). Importantly, altered expression of SRSF7 is associated with a vari-
109 ety of human cancers (Boguslawska et al., 2016; Cun et al., 2021; Fu and Wang, 2018; Song et
110 al., 2020; Xu et al., 2022).
111 In RAW MΦs lacking SRSF7, we identified a large cohort of genes whose expression
112 relied on SRSF7 at rest and after *Salmonella* infection. Curiously, in both conditions, many
113 SRSF7-impacted genes fell into the category of interferon stimulated genes (ISGs). After compu-
114 tational quantification of alternatively spliced genes ruled out a role for SRSF7 in mediating alter-
115 native splicing of ISG pre-mRNAs, we set out to elucidate the mechanism though which SRSF7
116 controls the type I IFN response in macrophages. Herein, we report a novel role for SRSF7 in
117 controlling the transcription of interferon responsive factor 7 (IRF7), a critical player in activating
118 the type I IFN response (Ning et al., 2011). Specifically, we demonstrate that SRSF7 enables
119 recruitment of signal transducer and activator of transcription 1 (STAT1) to the *Irf7* promoter and
120 relieves RNA polymerase II pausing. SRSF7 accomplishes this through interactions with the his-
121 tone methyltransferase KMT5a (a.k.a. SET8), which deposits H4K20me1 at the *Irf7* promoter fol-
122 lowing LPS treatment to maximize STAT1 association. By revealing a complex regulatory network
123 at the *Irf7* promoter that controls homeostatic and pathogen-induced type I interferon signaling,
124 our work identifies an unexpected mechanism through which SR proteins can orchestrate mac-
125 rophage innate immune gene expression and dictate infection outcomes.
126
127 **RESULTS**
128 **SRSF7-dependent alternative splicing is independent of macrophage activation state**

129 As differential phosphorylation of SRSF7 was detected over the course of *M. tuberculosis*
130 infection in macrophages (Budzik et al., 2020), we were motivated to examine how macrophage
131 activation might impact its function. To test the hypothesis that alternative splicing (AS) events
132 might be distinct between resting and activated macrophages, signifying functionalization of
133 SRSF7, we generated two *Srsf7* knockdown cell lines by transducing RAW MΦs (*Srsf7* KD #1
134 and *Srsf7* KD #2) with lentivirus containing shRNA hairpin constructs designed against the *Srsf7*
135 3'UTR and selected these cell lines alongside a scramble (SCR) control (**Fig. 1A-B**). RNA-seq
136 was performed comparing SCR and *Srsf7* knockdown (KD) #2 in two conditions: uninfected (UN)
137 or infected with the gram-negative bacterial pathogen *Salmonella enterica* serovar Typhimurium
138 (4h post-infection; +SAL). *Salmonella* induces robust innate immune responses in macrophages
139 though TLR4, which activates NFκB downstream of the MyD88 adapter and IRF3/IRF7 down-
140 stream of TRIF (Fitzgerald et al., 2003). Differential expression analysis was conducted using the
141 Qiagen CLC Genomics Workbench and quantification of alternative splicing changes was carried
142 out using MAJIQ (Modeling Alternative Junction Inclusion Quantification) (Vaquero-Garcia et al.,
143 2016). Consistent with SRSF7's designation as a splicing factor and previous studies implicating
144 it in alternative splicing specific pre-mRNAs (Gu et al., 2012; Kadota et al., 2020), we identified
145 1857 total SRSF7-dependent alternative splicing events in resting RAW MΦs and 1909 SRSF7-
146 dependent events in *Salmonella*-infected RAW MΦs (4h post-infection) (**Fig. 1C**) ($p<0.05$; >10%
147 PSI) (**Supplemental Table 1**). As expected for an SR protein that promotes exon recognition/in-
148 clusion, most changes were at the level of exon skipping. Of the 964 genes subject to SRSF7-
149 dependent alternative splicing in resting MΦs and the 993 genes in *Salmonella*-infected macro-
150 phages, 493 of these genes overlapped (**Fig. 1D**). Notably, only a handful of the detected alter-
151 native splicing changes occurred in genes that were also differentially expressed in *Srsf7* knock-
152 down macrophages, suggesting that *Srsf7* impacts steady state RNA levels in a splicing-inde-
153 pendent fashion (**Fig. 1E**).
154 Because our lists of alternatively spliced genes in resting and *Salmonella*-infected MΦs
155 did not completely overlap, we hypothesized that SRSF7 mediates distinct alternative splicing
156 events in the two MΦ states. To begin to test this, we prioritized a set of genes with the most
157 significant SRSF7-dependent AS changes (>20% PSI; confidence threshold 0.95) in each condi-
158 tion (UN and +SAL) (**Fig. S1A**). Manual annotation of these 36 genes did not reveal significant
159 enrichment for any functional category and none of the top alternative splicing events occurred in
160 genes with characterized roles in the MΦ innate immune response (**Fig. S1A**).
161 We first looked at SRSF7-dependent exon 6 skipping in *Dcun1d2* (Ensembl Transcript ID:
162 ENSMUST00000045366.10), a gene associated with Cullin neddylation (Kajigaya et al., 2016).

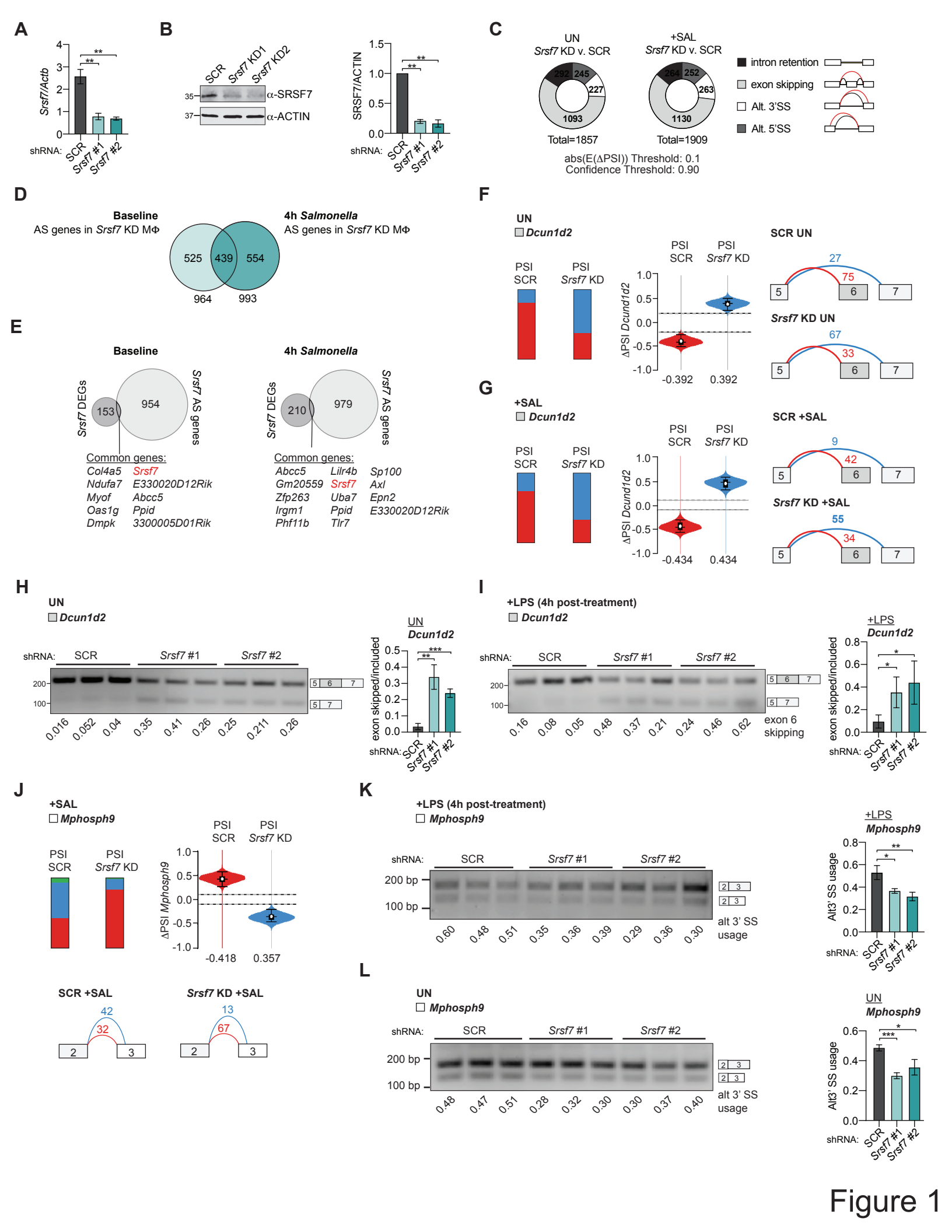
A
Srsf7/Actb
shRNA: SCR Srsf7 #1 Srsf7 #2
B
SCR Srsf7 KD1 Srsf7 KD2
α-SRSF7
α-ACTIN
SRSF7/ACTIN
C
UN
Srsf7 KD v. SCR
+SAL
Srsf7 KD v. SCR
Total=1857
Total=1909
intron retention
exon skipping
Alt. 3'SS
Alt. 5'SS
abs(E(ΔPSI)) Threshold: 0.1
Confidence Threshold: 0.90
D
Baseline
AS genes in Srsf7 KD MΦ
4h Salmonella
AS genes in Srsf7 KD MΦ
525 439 554
964 993
E
Baseline
4h Salmonella
Srsf7 DEGs
Srsf7 AS genes
153 954
210 979
Common genes:
Col4a5 Srsf7
Ndufa7 E330020D12Rik
Myof Abcc5
Oas1g Ppid
Dmpk 3300005D01Rik
Common genes:
Abcc5 Lilr4b Sp100
Gm20559 Srsf7 Axl
Zfp263 Uba7 Epn2
Irgm1 Ppid E330020D12Rik
Phf11b Tlr7
F
UN
Dcun1d2
PSI SCR
PSI Srsf7 KD
ΔPSI Dcund1d2
-0.392 0.392
SCR UN
Srsf7 KD UN
G
+SAL
Dcun1d2
-0.434 0.434
SCR +SAL
Srsf7 KD +SAL
H
UN
Dcun1d2
shRNA: SCR Srsf7 #1 Srsf7 #2
0.016 0.052 0.04 0.35 0.41 0.26 0.25 0.211 0.26
exon skipped/included
I
+LPS (4h post-treatment)
Dcun1d2
0.16 0.08 0.05 0.48 0.37 0.21 0.24 0.46 0.62
exon 6 skipping
J
+SAL
Mphosph9
ΔPSI Mphosph9
-0.418 0.357
SCR +SAL
Srsf7 KD +SAL
K
+LPS (4h post-treatment)
Mphosph9
200 bp
100 bp
0.60 0.48 0.51 0.35 0.36 0.39 0.29 0.36 0.30
alt 3' SS usage
Alt3' SS usage
L
UN
Mphosph9
0.48 0.47 0.51 0.28 0.32 0.30 0.30 0.37 0.40

Figure 1

Figure 1: Macrophage activation does not regulate SRSF7 control of alternative splicing

A. RT-qPCR of *Srsf7* in *Srsf7* KD RAW MΦs relative to SCR controls. **B.** Immunoblot of SRSF7 in shSCR, sh*Srsf7* #1, sh*Srsf7* #2 RAW MΦs. Right, quantification. **C.** Local splicing variations (AS) in *Srsf7* RAW MΦs compared to SCR at baseline (UN; left) and +*Salmonella* Typhimurium (4h) (+SAL; right). ∆PSI > 0.1 confidence threshold set at 0.90. **D.** Venn diagram of genes containing one or more AS event in UN vs. +SAL samples. **E.** Venn diagram of differentially expressed genes (DEGs) vs. alternatively spliced genes (AS) in UN and +SAL samples. **F.** MAJIQ PSI quantification of junctions with SCR (left) and *Srsf7* KD (right) in UN samples. Violin plot of ∆PSI *Dcun1d2* SRSF7-dependent local splicing variation. Splice graph of *Dcun1d2* in SCR (top) and *Srsf7* KD (bottom) generated by MAJIQ/VOILA **G.** As in F but for +SAL samples. **H.** Semi-quantitative RT-PCR of *Dcun1d2* in SCR, *Srsf7* KD #1 and KD #2 RAW MΦs. Each sample in biological triplicate. Right, quantification. **I.** As in H but for *Dcun1d2* +LPS (4h) **J.** As in F but *Mphosph9.* **K.** As in H but *Mphosph9* (+4h LPS). **L.** As in H but *Mphosph9* in UN samples. Data are expressed as a mean of three or more biological replicates with error bars depicting SEM. Statistical significance was determined using two tailed unpaired student's t test. *=p<0.05, **=p<0.01, ***=p<0.001.

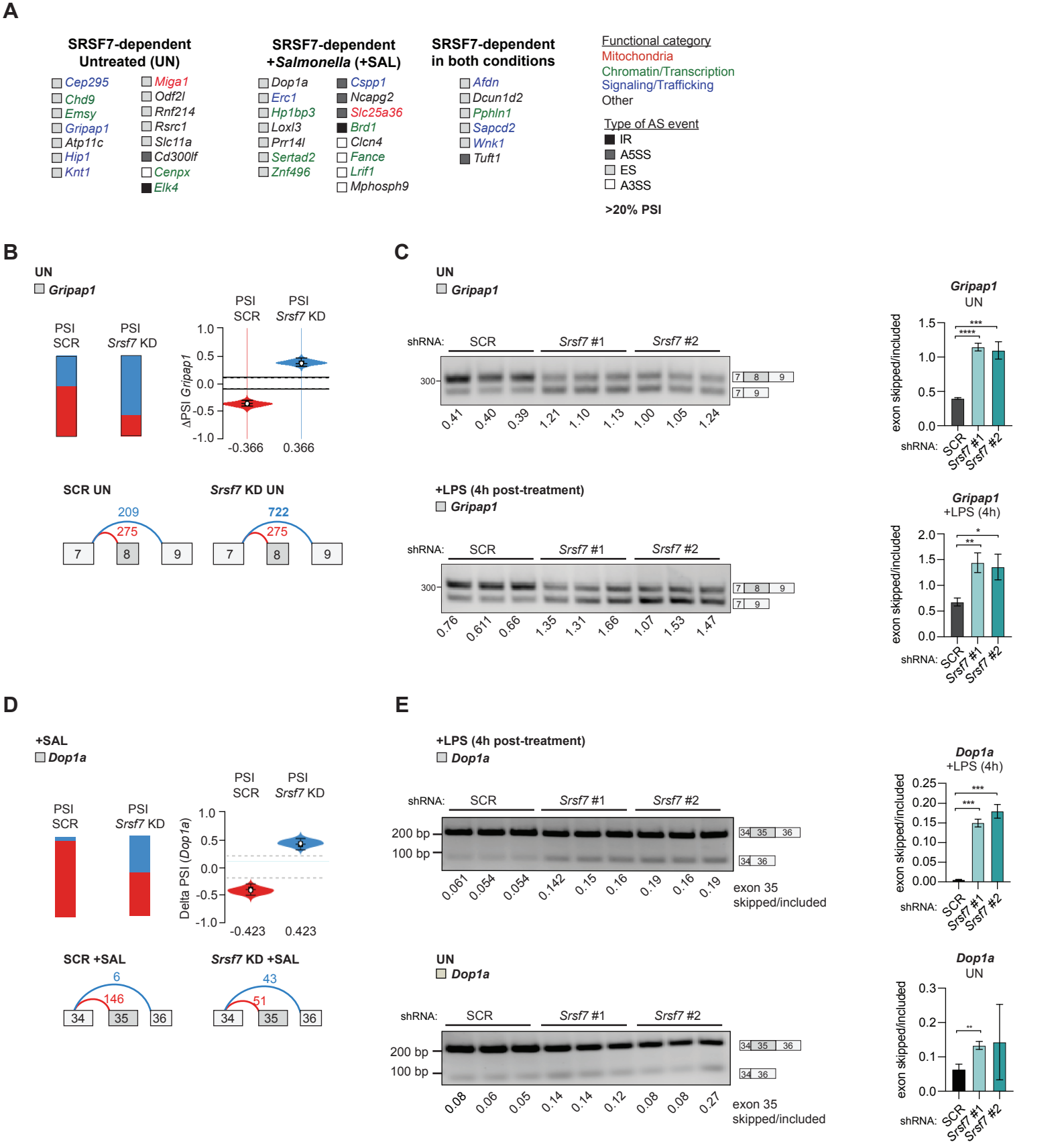
A
SRSF7-dependent Untreated (UN)
Cep295
Chd9
Emsy
Gripap1
Atp11c
Hip1
Knt1
Miga1
Odf2l
Rnf214
Rsrc1
Slc11a
Cd300lf
Cenpx
Elk4
SRSF7-dependent +Salmonella (+SAL)
Dop1a
Erc1
Hp1bp3
Loxl3
Prr14l
Sertad2
Znf496
Cspp1
Ncapg2
Slc25a36
Brd1
Clcn4
Fance
Lrif1
Mphosph9
SRSF7-dependent in both conditions
Afdn
Dcun1d2
Pphln1
Sapcd2
Wnk1
Tuft1
Functional category
Mitochondria
Chromatin/Transcription
Signaling/Trafficking
Other
Type of AS event
IR
A5SS
ES
A3SS
>20% PSI
B
UN
Gripap1
PSI SCR
PSI Srsf7 KD
ΔPSI Gripap1
-0.366
0.366
SCR UN
Srsf7 KD UN
209
275
722
275
C
UN
Gripap1
shRNA: SCR Srsf7 #1 Srsf7 #2
0.41 0.40 0.39 1.21 1.10 1.13 1.00 1.05 1.24
+LPS (4h post-treatment)
Gripap1
0.76 0.611 0.66 1.35 1.31 1.66 1.07 1.53 1.47
exon skipped/included
D
+SAL
Dop1a
Delta PSI (Dop1a)
-0.423
0.423
SCR +SAL
Srsf7 KD +SAL
6
146
43
51
E
+LPS (4h post-treatment)
Dop1a
200 bp
100 bp
0.061 0.054 0.054 0.142 0.15 0.16 0.19 0.16 0.19
exon 35 skipped/included
UN
0.08 0.06 0.05 0.14 0.14 0.12 0.08 0.08 0.27

Figure S1: Supplemental data for Figure 1

A. Functional categorization of alternatively spliced transcripts in *Srsf7* knockdown RAW MΦs vs. SCR (UN, +SAL, and ∆PSI > 0.2 confidence threshold set at 0.95. **B.** MAJIQ PSI quantification of *Gripap1* junctions with SCR (left) and *Srsf7* KD (right). Violin plot of ∆PSI *Gripap1* SRSF7-dependent local splicing variation. Splice graph of *Gripap1* in SCR (bottom left) and *Srsf7* KD (bottom right) generated by MAJIQ/VOILA at baseline. **C.** Semiquantitative PCR of *Gripap1* in SCR, *Srsf7* KD1 and KD2 RAW MΦs, UN (top) and 4h +LPS (bottom). Each sample in biological triplicate. Right, quantification. **D.** MAJIQ PSI quantification of *Dop1a* junctions with SCR (left) and *Srsf7* KD (right). Violin plot of ∆PSI *Dop1a* SRSF7-dependent local splicing variation. Splice graph of *Dop1a* in SCR (bottom left) and *Srsf7* KD (bottom right) generated by MAJIQ/VOILA at baseline. **E** Semiquantitative PCR of *Gripap1* in SCR, *Srsf7* KD #1 and KD #2 RAW MΦs, 4h +LPS (top) and UN (bottom). Each sample in biological triplicate. Right, quantification. Data are expressed as a mean of three biological replicates with error bars depicting SEM. Statistical significance was determined using two tailed unpaired student's t test. *=p<0.05, **=p<0.01, ***=p<0.001, ****=p<0.0001.

163 MAJIQ measured significant enrichment of this exon skipping event in both untreated and *Salmo-*
164 *nella*-infected *Srsf7* knockdown MΦs (ΔPSI 39.2% in UN and 43.4% in +SAL) (**Fig. 1F-G**). We
165 confirmed this via semi-quantitative RT-PCR using RNA isolated from uninfected MΦs and MΦs
166 treated with lipopolysaccharide (LPS). LPS activates TLR4 in MΦs in a manner analogous to
167 *Salmonella* infection but provides tighter kinetic control experimentally. Consistent with our MAJIQ
168 analysis, we measured significantly higher levels of *Dcun1d2* exon 6 skipping in *Srsf7* knockdown
169 MΦs in both conditions (**Fig. 1H-I**).
170 Next, we looked at an alternative splicing event computationally predicted to be "activa-
171 tion-dependent" (i.e. only detected in +SAL MΦs) (**Fig. 1D**). In +SAL samples, MAJIQ quantified
172 SRSF7-dependent alternative 3'SS usage in exon 3 of the *Mphosph9* gene (Ensembl Transcript
173 ID: ENSMUST00000184951.8), which encodes an M-phase phosphoprotein (*Srsf7* knockdown
174 #2 (ΔPSI -35.7%) (**Fig. 1J**)). Again, by RT-PCR, we confirmed that this event occurs preferentially
175 in *Srsf7* knockdown MΦs (**Fig. 1K**). Curiously however, we also measured preferential alternative
176 3'SS usage in untreated *Srsf7* knockdown MΦs (**Fig. 1L**), even though this event was not com-
177 putationally identified by RNA-seq/MAJIQ. Similarly, SRSF7-dependent inclusion of exon 8 in
178 *Gripap1* (Ensembl Transcript ID ENSMUST00000065932.14) (**Fig. S1B**), and inclusion of exon
179 35 in *Dop1a* (Ensembl Transcript ID ENSMUST00000190957.7) (**Fig. S1D)** only met our thresh-
180 old in UN and +SAL conditions, respectively, but could be detected in both macrophage states by
181 RT-PCR (**Fig. S1C, S1E**). These data argue that although SRSF7 is important for making alter-
182 native splicing decisions in RAW MΦs, it largely mediates the same events in the presence and
183 absence of LPS. Based on the nature of the genes whose alternative splicing relies on SRSF7
184 and the lack of specificity for alternative splicing in resting vs. activated MΦs, we can conclude
185 that SRSF7 does not dramatically influence the macrophage innate immune transcriptome at the
186 level of splicing.
187
188 **SRSF7 is a positive regulator of interferon stimulated genes (ISGs) in macrophages**
189 In addition to the alternative splicing events reported in Fig. 1, we also measured hundreds
190 of differentially expressed genes in resting and *Salmonella*-infected *Srsf7* knockdown RAW MΦs
191 compared to controls (**Supplementary Table 2**). In resting MΦs, *Srsf7* knockdown impacted ex-
192 pression of many housekeeping genes in resting MΦs, particularly in pathways related to transla-
193 tion regulation (EIF2 signaling and Regulation of eIF4 and p70S6K signaling) and phagosome
194 maturation (**Fig. S2A**). Interestingly, in resting MΦs, we also noted enrichment for SRSF7-de-
195 pendent genes in pathways like "Communication between innate and adaptive immune cells"

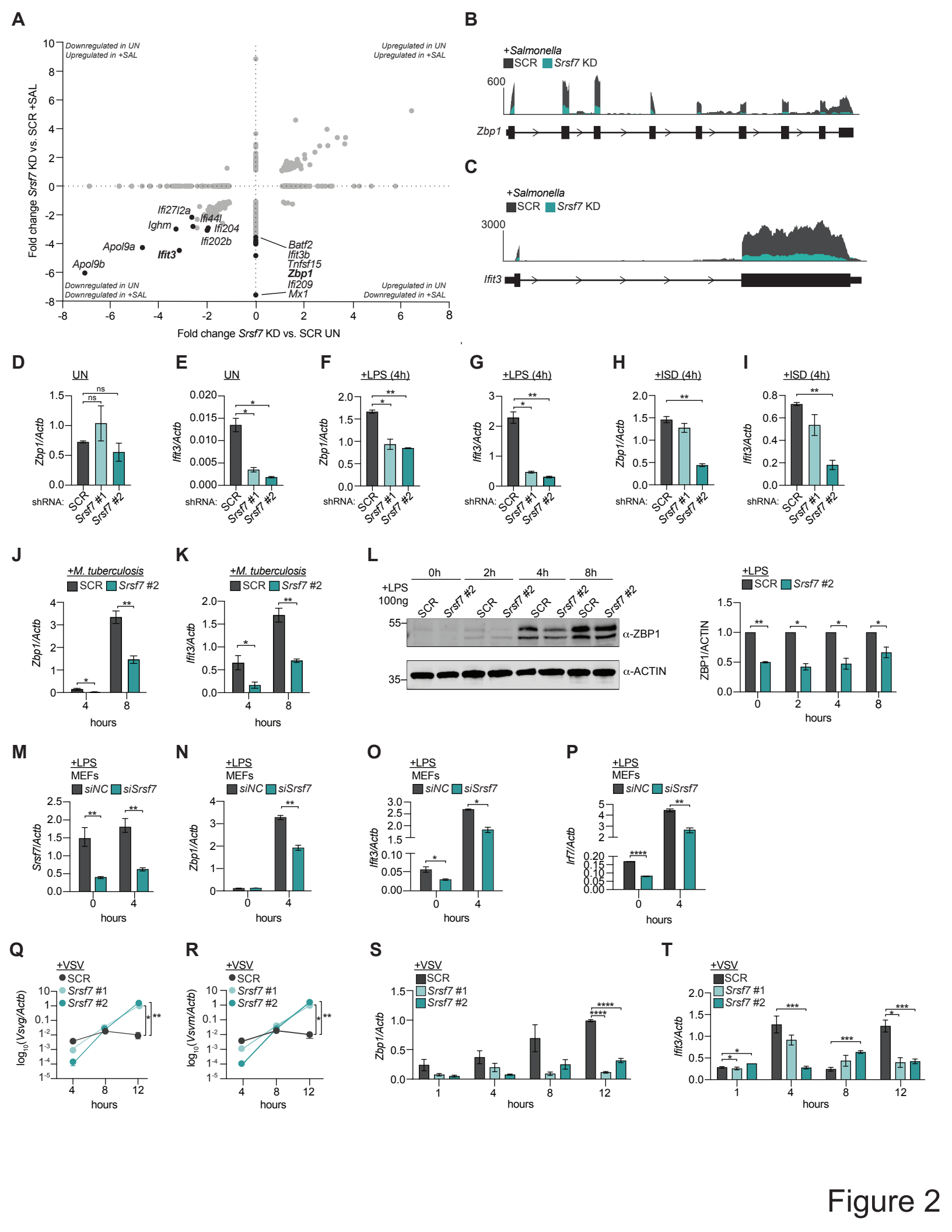
A
Downregulated in UN
Upregulated in +SAL
Upregulated in UN
Upregulated in +SAL
Downregulated in UN
Downregulated in +SAL
Upregulated in UN
Downregulated in +SAL
Fold change Srsf7 KD vs. SCR +SAL
Fold change Srsf7 KD vs. SCR UN
Ifi27l2a
Ifi44l
Ighm
Ifi204
Ifi202b
Apol9a
Ifit3
Apol9b
Batf2
Ifit3b
Tnfsf15
Zbp1
Ifi209
Mx1
B
+Salmonella
SCR
Srsf7 KD
600
Zbp1
C
+Salmonella
SCR
Srsf7 KD
3000
Ifit3
D
UN
Zbp1/Actb
shRNA:
SCR
Srsf7 #1
Srsf7 #2
ns
E
UN
Ifit3/Actb
F
+LPS (4h)
Zbp1/Actb
G
+LPS (4h)
Ifit3/Actb
H
+ISD (4h)
Zbp1/Actb
I
+ISD (4h)
Ifit3/Actb
J
+M. tuberculosis
SCR
Srsf7 #2
Zbp1/Actb
hours
K
+M. tuberculosis
SCR
Srsf7 #2
Ifit3/Actb
hours
L
0h
2h
4h
8h
+LPS
100ng
SCR
Srsf7 #2
55
35
α-ZBP1
α-ACTIN
+LPS
SCR
Srsf7 #2
ZBP1/ACTIN
hours
M
+LPS
MEFs
siNC
siSrsf7
Srsf7/Actb
hours
N
+LPS
MEFs
siNC
siSrsf7
Zbp1/Actb
hours
O
+LPS
MEFs
siNC
siSrsf7
Ifit3/Actb
hours
P
+LPS
MEFs
siNC
siSrsf7
Irf7/Actb
hours
Q
+VSV
SCR
Srsf7 #1
Srsf7 #2
log10(Vsvg/Actb)
hours
R
+VSV
SCR
Srsf7 #1
Srsf7 #2
log10(Vsvm/Actb)
hours
S
+VSV
SCR
Srsf7 #1
Srsf7 #2
Zbp1/Actb
hours
T
+VSV
SCR
Srsf7 #1
Srsf7 #2
Ifit3/Actb
hours

Figure 2

623 **Figure 2: SRSF7 promotes the type I interferon response**

624

625 **A.** Scatterplot of genes differentially expressed in *Srsf7* KD RAW MΦs relative to SCR in each of
626 the conditions queried (X axis = UN; Y axis = +SAL). Select interferon stimulated genes depicted
627 in black. **B.** Integrated Genomics Viewer track of *Zbp1* SCR (grey) and *Srsf7* KD (teal) reads from
628 *Salmonella*-infected cells. **C.** As in B but for *Ifit3.* **D.** RT-qPCR of *Zbp1* in SCR, *Srsf7* KD#1, and
629 *Srsf7* KD#2 RAW MΦs at baseline (UN). **E.** As in D but for *Ifit3.* **F.** RT-qPCR of *Zbp1* in SCR,
630 *Srsf7* KD#1, and *Srsf7* KD#2 RAW MΦs 4h post-stimulation with 100 ng/ml LPS. **G.** As in F but
631 for *Ifit3.* **H.** RT-qPCR of *Zbp1* in SCR, *Srsf7* KD#1, and *Srsf7* KD#2 RAW MΦs 4h post-transfection
632 with 1 µg/ml ISD. **I.** As in F but for *Ifit3.* **J.** RT-qPCR of *Zbp1* in SCR and *Srsf7* KD #2 RAW MΦs
633 at 4 and 8h post-infection with *M. tuberculosis* (Erdman strain; MOI=5). **K.** As in J but for *Ifit3.* **L.**
634 Immunoblot of ZBP1 protein levels in SCR and *Srsf7* KD #2 RAW MΦs at baseline, 4, and 8h,
635 post-stimulation with 100 ng/ml LPS. Right, quantification. **M.** RT-qPCR of *Srsf7* in primary MEFs
636 at baseline or 4h post stimulation with 100ng LPS. **N.** As in M but for *Zbp1*. **O.** As in M but for *Ifit3*.
637 **P.** As in M but for *Irf7*. **Q.** RT-qPCR of *Vsvg* in SCR, *Srsf7* KD #1, and *Srsf7* KD #2 RAW MΦs at
638 4, 8, 12h post-infection with VSV (MOI=0.1). **R.** As in M but for *Vsvm.* **S.** RT-qPCR of *Zbp1* in
639 SCR, *Srsf7* KD #1, *Srsf7* KD #2 RAW MΦs at 1, 4, 8, 12h post-infection with VSV (MOI=0.1). **T.**
640 As in S but for *Ifit3.* Data are expressed as a mean of three biological replicates with error bars
641 depicting SEM. Statistical significance was determined using two tailed unpaired student's t test.
642 *=p<0.05, **=p<0.01, ***=p<0.001, ****=p<0.0001.

643
644
645
646
647
648
649
650
651
652
653
654
655
656

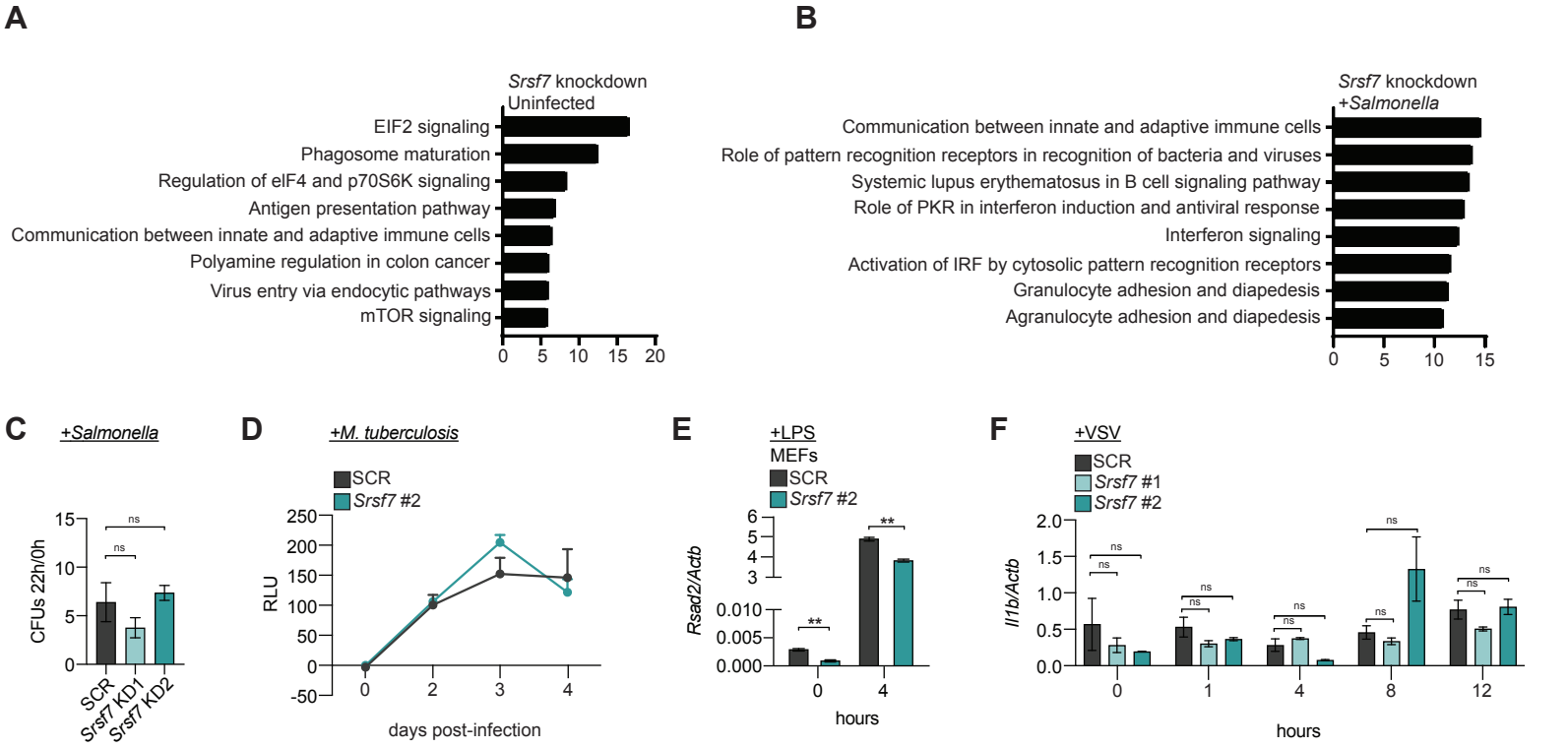
A
Srsf7 knockdown
Uninfected
EIF2 signaling
Phagosome maturation
Regulation of eIF4 and p70S6K signaling
Antigen presentation pathway
Communication between innate and adaptive immune cells
Polyamine regulation in colon cancer
Virus entry via endocytic pathways
mTOR signaling
0 5 10 15 20
B
Srsf7 knockdown
+Salmonella
Communication between innate and adaptive immune cells
Role of pattern recognition receptors in recognition of bacteria and viruses
Systemic lupus erythematosus in B cell signaling pathway
Role of PKR in interferon induction and antiviral response
Interferon signaling
Activation of IRF by cytosolic pattern recognition receptors
Granulocyte adhesion and diapedesis
Agranulocyte adhesion and diapedesis
0 5 10 15
C
+Salmonella
CFUs 22h/0h
ns
ns
SCR
Srsf7 KD1
Srsf7 KD2
D
+M. tuberculosis
SCR
Srsf7 #2
RLU
days post-infection
E
+LPS
MEFs
SCR
Srsf7 #2
Rsad2/Actb
**
**
hours
F
+VSV
SCR
Srsf7 #1
Srsf7 #2
Il1b/Actb
ns
hours

S2

Figure S2: Supplemental data for Figure 2

A. Ingenuity Pathway Analysis (IPA; Qiagen) of pathways enriched for differentially expressed genes in *Srsf7* KD RAW MΦs (UN). **B.** As in A for *Srsf7* KD RAW MΦs +SAL. **C.** Infection of SCR and *Srsf7* KD RAW MΦs with *Salmonella* enterica (MOI=1) in non-SPI-1 inducing conditions. Fold-replication represented as 22h over 2h post-infection. **D.** Mtb luxBCADE growth in SCR or *Srsf7* KD RAW MΦs measured by relative light units (RLUs) over a 4-day time course (MOI=1). **E.** RT-qPCR of *Rsad2* in siRNA *Srsf7*- or siControl-transfected primary MEFs at baseline or 4h post stimulation with 100ng/ml of LPS. **F.** RT-qPCR of *Il1b* in SCR or *Srsf7* KD RAW MΦs over a time course of VSV infection. Data are expressed as a mean of three or more biological replicates with error bars depicting SEM. Statistical significance was determined using two tailed unpaired student's t test. *=$p<0.05$, **=$p<0.01$.

196 (**Fig. S2A**), suggesting that loss of SRSF7 dysregulates innate immune gene expression even in
197 the absence of a stimulus.

198 Enrichment for pathways related to innate immunity was also evident in *Salmonella*-in-
199 fected macrophages, where knockdown of *Srsf7* dysregulated genes in pathways related to "role
200 of pattern recognition receptors in recognition of bacteria and viruses," "interferon signaling," "role
201 of PKR in interferon induction and antiviral response," and "activation of IRF by cytosolic pattern
202 recognition receptors" (**Fig. S2B**). Many of these categories contain genes related to the type I
203 interferon (IFN) response, a ubiquitous antiviral response characterized by expression of inter-
204 feron alpha and beta and interferon stimulated genes (ISGs) (Schoggins, 2019; Schoggins and
205 Rice, 2011). In MΦs, the type I IFN response is activated by the transcription factors IRF3 and
206 IRF7 in response to several immune agonists including LPS/*Salmonella* infection, cytosolic
207 dsDNA, and cytosolic dsRNA (Honda and Taniguchi, 2006; Jefferies, 2019; Schoggins et al.,
208 2011).

209 For ISGs that are appreciably expressed in resting MΦs (Barrat et al., 2019; Gough et al.,
210 2012), e.g. *Apol9a*, *Apol9b*, *Ifit3*, and *Ifi202b*, *Srsf7* knockdown decreased their abundance in
211 both untreated and +*Salmonella* conditions (**Fig. 2A**; bottom left quadrant). Genes like *Mx1, Zbp1,*
212 and *Ifi209*, which are virtually undetectable in resting cells, only displayed SRSF7-dependence in
213 our *Salmonella*-infected samples (**Fig. 2A**; lower y-axis). Visualizing RNA reads from *Srsf7* knock-
214 down versus control MΦs for two such ISGs, *Zbp1* and *Ifit3*, on the Integrated Genomics Viewer,
215 revealed no changes in intronic reads (**Fig. 2B-C**). This was consistent with our MAJIQ analysis,
216 which did not detect many statistically significant splicing changes in genes annotated as ISGs in
217 *Srsf7* knockdown RAW MΦs (**Fig. 1E, Supplemental Table 1)**.

218 Failure to phagocytose *Salmonella* or defects in *Salmonella* replication could result in
219 lower ISG expression in *Srsf7* knockdown cells, but enumeration of colony forming units (CFUs)
220 did not reveal any differences in bacterial burdens between SCR and *Srsf7* knockdown RAW MΦs
221 over a 22h infection time-course (**Fig. S2C**). To determine if SRSF7's ability to promote ISG ex-
222 pression was unique to *Salmonella* infection, we measured ISG expression in SCR and *Srsf7*
223 knockdown MΦs at 4h post-treatment with LPS (100 ng/ml), after dsDNA transfection, which ac-
224 tivates type I IFN gene expression downstream of cGAS (1 μg ISD), and after treatment with
225 recombinant IFN-β, which activates ISG expression in MΦs by binding to IFNAR and engaging
226 JAK/STAT cascades (200 IU, 4h). In all cases, loss of *Srsf7* led to impaired activation of *Zbp1*
227 and *Ifit3* expression (**Fig. 2D-I**). We also measured lower ISG expression in *Srsf7* knockdown
228 MΦs during infection with the intracellular bacterial pathogen, *Mycobacterium tuberculosis* (MOI
229 = 5) (**Fig. 2J-K**), which elicits *Ifnb1* and ISG expression via the cGAS/STING pathway (Watson et

230 al., 2015). Again, this defect in ISG expression was independent of bacterial internalization/repli-
231 cation (**Fig. S2D**). Over an 8h time-course of LPS-treatment, lower *Zbp1* transcript levels corre-
232 lated with lower protein accumulation (**Fig. 2L**), suggesting that failure to fully upregulate ISG
233 expression in *Srsf7* knockdown MΦs is likely to functionally impact the innate immune response
234 to infection. This phenotype was not unique to RAW MΦs, as siRNA knockdown of SRSF7 in
235 primary mouse embryonic fibroblasts (MEFs)(**Fig. 2M**), a cell type commonly used for studies of
236 type I interferon signaling, also resulted in low basal ISG expression and a failure to fully induce
237 ISGs upon LPS stimulation (**Fig. 2N-P and S2E)**.
238 To test whether SRSF7 is a *bona fide* player in activating antimicrobial immunity in MΦs,
239 we infected SCR and *Srsf7* knockdown MΦs with vesicular stomatitis virus (VSV), a negative-
240 strand RNA virus that stimulates type I IFN responses via TLR3 and RIG-I and is extremely sen-
241 sitive to ISG expression (Gao et al., 2021; Wagner et al., 2021). We measured a dramatic increase
242 in VSV replication in *Srsf7* knockdown MΦs, measured by RT-qPCR of two VSV genes, *Vsvg* and
243 *Vsvm* (**Fig. 2Q-R**), that was concomitant with depressed ISG transcript induction over a 12-hour
244 time course of VSV infection (MOI = 0.1) (**Fig. 2S-T**). We did not detect SRSF7-dependent differ-
245 ences in *Il1b* expression in response to VSV infection, arguing against a role for SRSF7 in con-
246 trolling innate gene expression downstream of NFκB (**Fig. S2F**). Together, these data identify
247 SRSF7 as a positive regulator of the type I IFN response in MΦs and suggest that the mechanism
248 of SRSF7-dependent ISG expression is shared by several pathogen sensing cascades (i.e. oc-
249 curs at one or more nodes where the TLR4, cGAS, and RIG-I cascades converge).
250
251 **SRSF7 drives ISG expression by promoting expression of the transcription factor IRF7**
252 Given that loss of SRSF7 results in a failure to fully induce many ISGs, we hypothesized
253 that SRSF7 may act directly on one or more critical innate signaling proteins or transcription fac-
254 tors. To pinpoint where in the type I IFN signaling response SRSF7 acts, we treated *Srsf7*
255 knockdown or SCR RAW MΦs with LPS (100 ng/ml) and measured secretion of type I interferon
256 (IFN-β/α) over a 6h time-course via an ISRE-luciferase reporter cell line (Hoffpauir et al., 2020;
257 Wagner et al., 2022). *Srsf7* knockdown MΦs produced significantly less IFN-β/α compared to
258 SCR controls at all time points measured (**Fig. 3A**). We next asked if impaired ISG expression
259 in *Srsf7* knockdown MΦs could be rescued if *Srsf7* knockdown and SCR control cells received
260 equal amounts of recombinant IFN-β. We found that even post treatment of IFN-β, *Srsf7* knock-
261 down MΦs fail to express ISGs like *Ifi202b* and *Zbp1* to the same level as SCR controls, at both
262 the transcript (**Fig. 3B-C**) and protein level (**Fig. 3D**). These results suggest that loss of SRSF7
263 impacts some aspect of the type I IFN response that is engaged upstream and downstream of

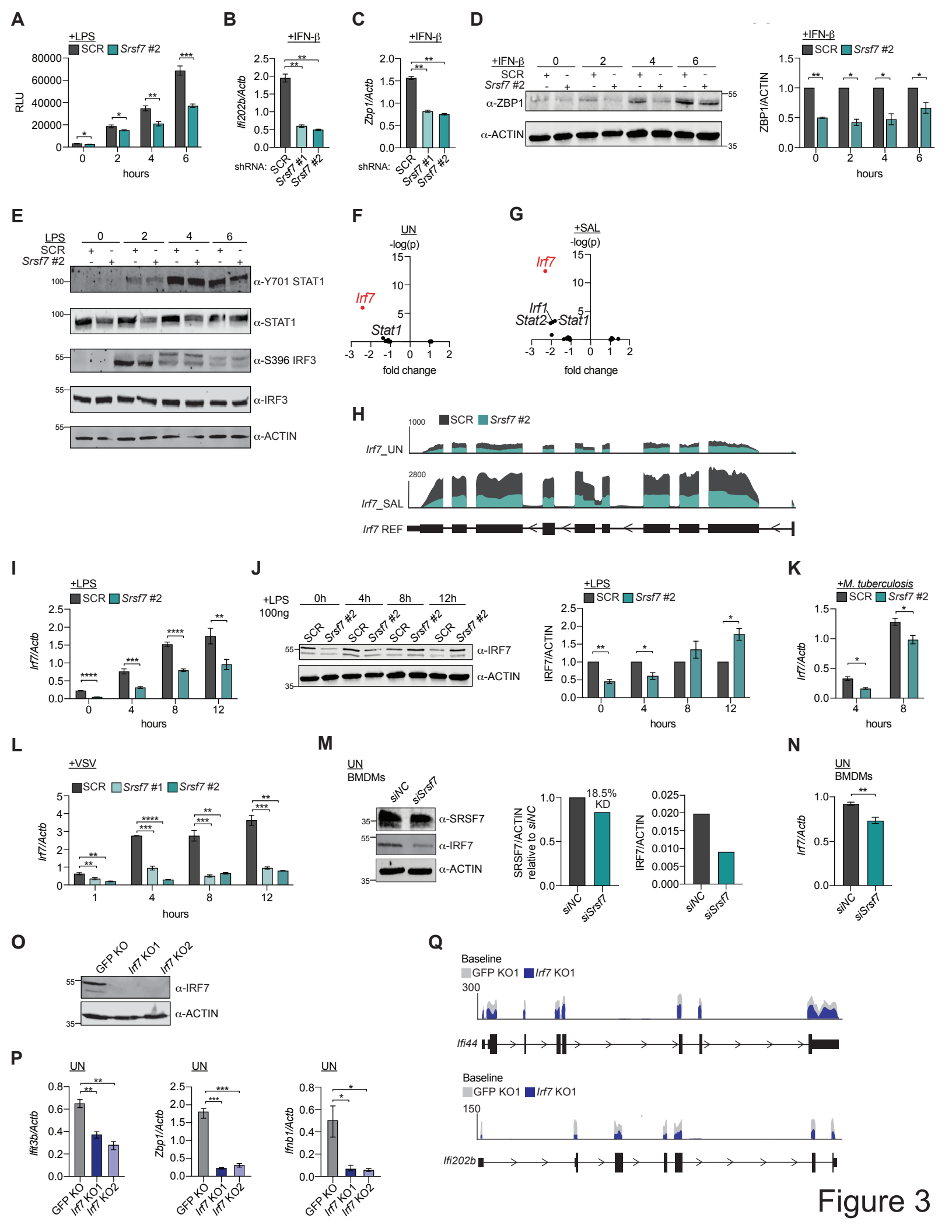
A
+LPS
SCR
Srsf7 #2
RLU
hours
B
+IFN-β
Ifi202b/Actb
shRNA:
SCR
Srsf7 #1
Srsf7 #2
C
+IFN-β
Zbp1/Actb
D
+IFN-β
α-ZBP1
α-ACTIN
ZBP1/ACTIN
E
LPS
α-Y701 STAT1
α-STAT1
α-S396 IRF3
α-IRF3
α-ACTIN
F
UN
-log(p)
Irf7
Stat1
fold change
G
+SAL
Irf7
Irf1
Stat2
Stat1
H
SCR
Srsf7 #2
Irf7_UN
Irf7_SAL
Irf7 REF
I
+LPS
Irf7/Actb
J
+LPS
100ng
0h
4h
8h
12h
α-IRF7
α-ACTIN
IRF7/ACTIN
K
+M. tuberculosis
L
+VSV
Srsf7 #1
M
UN
BMDMs
siNC
siSrsf7
α-SRSF7
SRSF7/ACTIN relative to siNC
18.5% KD
N
O
GFP KO
Irf7 KO1
Irf7 KO2
P
Ifit3b/Actb
Zbp1/Actb
Ifnb1/Actb
Q
Baseline
Ifi44
Ifi202b

Figure 3

691 **Figure 3: SRSF7 is required for IRF7 accumulation in macrophages**

692

693 **A.** Secreted IFNα/β in SCR and *Srsf7* KD#2 RAW MΦs, as a measure of luciferase expressed by
694 ISRE reporter cells. **B.** RT-qPCR of *Ifi202b* in SCR, *Srsf7* KD#1 and *Srsf7* KD#2 in RAW MΦs 4h
695 post-stimulation with 200 IU IFN-β. **C.** As in B for *Zbp1.* **D.** Immunoblot of ZBP1 and ACTIN over
696 a time course of IFN-β (200 IU) treatment in SCR and *Srsf7* KD#2 RAW MΦs. Quantification,
697 right. **E.** Immunoblot of Y701 STAT1, STAT1, S396 IRF3, IRF3, and ACTIN in SCR and *Srsf7* KD
698 RAW MΦs over a time course of LPS treatment (100 ng/ml). **F.** Differential expression of tran-
699 scription factor genes in untreated *Srsf7* knockdown vs. SCR RAW MΦs as fold change and -
700 log(p-value). Gene of interest (*Irf7*) highlighted in red. **G.** As in F but for +SAL samples. **H.** Inte-
701 grated Genomics Viewer with *Irf7* reads from SCR (grey) and *Srsf7* KD#2 (teal) RAW MΦs, un-
702 treated (top) and +*Salmonella* (bottom). **I.** RT-qPCR of *Irf7* over a time course of LPS stimulation
703 (100 ng/ml) in SCR and *Srsf7* KD RAW MΦs. **J.** Immunoblot of IRF7 and ACTIN protein levels
704 over a time course of LPS stimulation (100 ng/ml) in SCR and *Srsf7* KD RAW MΦs. Quantification,
705 right. **K.** RT-qPCR of *Irf7* over a time course of Mtb infection (Erdman strain; MOI=5) in SCR and
706 *Srsf7* KD#2 MΦs. **L.** RT-qPCR of *Irf7* over a time course of VSV infection (MOI=0.1) in SCR, *Srsf7*
707 KD#1, *Srsf7* KD#2 RAW MΦs. **M.** Immunoblot of SRSF7, IRF7, and ACTIN in siControl- or si*Srsf7*-
708 transfected BMDMs at baseline. Quantifications, right. **N.** RT-qPCR of *Irf7* in siControl or si*Srsf7*
709 BMDMs at baseline. **O.** Immunoblot of IRF7 protein levels in GFP gRNA, *Irf7* KO1 and *Irf7* KO2
710 RAW MΦs at baseline. ACTIN used as loading control. **P.** RT-qPCR of *Ifit3b, Zbp1,* or *Ifnb1* at
711 baseline in *Irf7* KO1 (blue) vs. GFP gRNA control (grey) RAW MΦs. **Q.** Integrated Genomics
712 Viewer with *Ifi44* and *Ifi202b* reads from GFP gRNA (grey) or *Irf7* KO (blue) RAW MΦs at baseline
713 (UN). Data expressed as a mean of three biological replicates with error bars depicting SEM
714 unless otherwise noted. Statistical significance was determined using two tailed unpaired stu-
715 dent's t test. *=p<0.05, **=p<0.01, ***=p<0.001, ****=p<0.0001.

716

717

718

719

720

721

722

723

724

264 IFNAR and that loss of IFN-β production is not the sole driver of ISG defects in *Srsf7* knock-
265 down MΦs.
266 We then asked whether altered signaling downstream of TLR4 could explain defective
267 ISG expression in *Srsf7* knockdown RAW MΦs. We treated *Srsf7* knockdown and SCR RAW
268 MΦs with LPS and measured phosphorylation of the transcription factor IRF3 (activated down-
269 stream of TLR4-TRIF signaling) and STAT1 (activated downstream of IFNAR) over a 6h time
270 course. We did not measure significant changes in phosphorylation of IRF3 at S396 or phos-
271 phorylation of STAT1 at Y701 (**Fig. 3E**; quantification in **Fig. S3A**), effectively ruling out defec-
272 tive signal transduction as the culprit for dampened ISG expression in *Srsf7* knockdown MΦs.
273 Next, we entertained the possibility that SRSF7 is required for the expression of one or
274 more transcription factors needed to activate the type I IFN response downstream of pattern
275 recognition receptor and/or IFNAR engagement. To test this, we generated a list of transcription
276 factors associated with macrophage innate immunity in the STAT, IRF, and NFκB families, and
277 turned back to our RNA-seq data to see how expression of each factor was impacted by loss of
278 SRSF7. While expression of most transcription factors was unaffected, we observed a signifi-
279 cant defect in *Irf7* expression in *Srsf7* knockdown RAW MΦs at baseline and after *Salmonella*
280 infection (**Fig. 3F-G**). Visualization of *Irf7* gene expression data on the IGV highlights fewer *Irf7*
281 exonic reads in *Srsf7* knockdown (teal) compared to SCR (grey) RAW MΦs in both conditions
282 (**Fig. 3H**). We did not detect an increase in intron reads in *Srsf7* knockdown MΦs nor did our
283 MAJIQ analysis identify SRSF7-dependent *Irf7* alternative splicing events (**Fig. 1D**), arguing
284 against a role for SRSF7 in regulating *Irf7* transcript abundance via splicing.
285 Initially discovered in the context of Epstein Barr virus, IRF7 (interferon regulatory factor
286 7) is a master regulator of antiviral type I IFN responses (Honda et al., 2005). Importantly, IRF7
287 is itself an ISG whose expression is induced downstream of IFNAR engagement. Although ba-
288 sal levels of IRF7 vary between immune cell types, we know that dendritic cells are heavily reli-
289 ant upon IRF7 at baseline and several studies have implicated IRF7 in priming early responses
290 in macrophages downstream of LPS (Fitzgerald et al., 2003; Gu et al., 2022; Jefferies, 2019;
291 Sin et al., 2020). We can readily measure IRF7 transcript and protein in resting wild-type RAW
292 MΦs (**Fig. 3I-J**) and in wild-type immortalized BMDMs (**Fig. S3B**), confirming their utility for
293 studies of IRF7 in resting and activated states. IRF7 protein levels are low in WT resting
294 BMDMs and are upregulated in response to LPS (**Fig. S3C**).
295 To better appreciate the kinetics of SRSF7-dependent control of *Irf7* expression, we
296 treated *Srsf7* knockdown and SCR control RAW MΦs with LPS and measured *Irf7* transcript and
297 protein over a 12h time course. Levels of *Irf7* mRNA were significantly lower in *Srsf7* knockdown

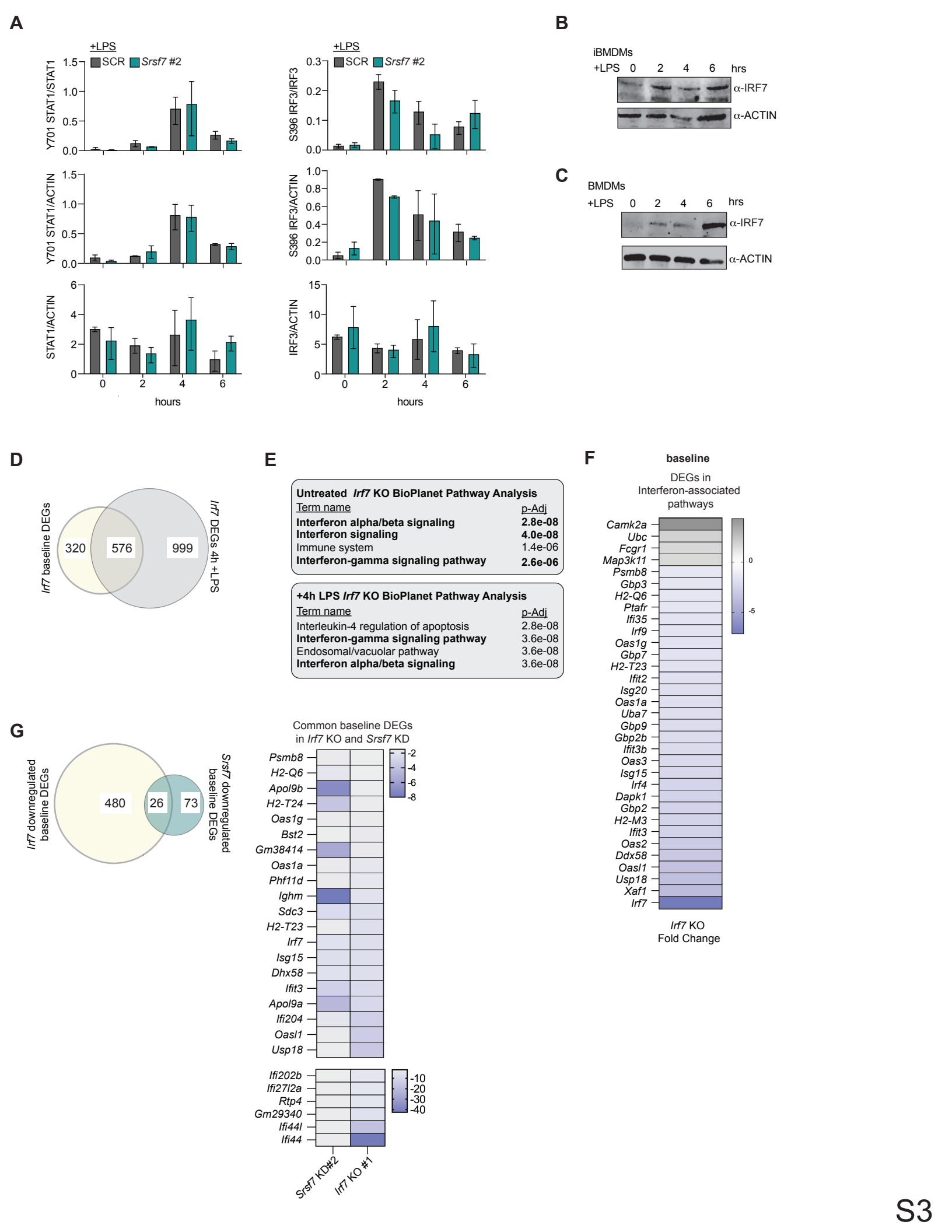
A
+LPS
SCR
Srsf7 #2
Y701 STAT1/STAT1
S396 IRF3/IRF3
Y701 STAT1/ACTIN
S396 IRF3/ACTIN
STAT1/ACTIN
IRF3/ACTIN
hours
B
iBMDMs
+LPS 0 2 4 6 hrs
α-IRF7
α-ACTIN
C
BMDMs
+LPS 0 2 4 6 hrs
α-IRF7
α-ACTIN
D
Irf7 baseline DEGs
Irf7 DEGs 4h +LPS
320
576
999
E
Untreated Irf7 KO BioPlanet Pathway Analysis
Term name p-Adj
Interferon alpha/beta signaling 2.8e-08
Interferon signaling 4.0e-08
Immune system 1.4e-06
Interferon-gamma signaling pathway 2.6e-06
+4h LPS Irf7 KO BioPlanet Pathway Analysis
Term name p-Adj
Interleukin-4 regulation of apoptosis 2.8e-08
Interferon-gamma signaling pathway 3.6e-08
Endosomal/vacuolar pathway 3.6e-08
Interferon alpha/beta signaling 3.6e-08
F
baseline
DEGs in Interferon-associated pathways
Camk2a
Ubc
Fcgr1
Map3k11
Psmb8
Gbp3
H2-Q6
Ptafr
Ifi35
Irf9
Oas1g
Gbp7
H2-T23
Ifit2
Isg20
Oas1a
Uba7
Gbp9
Gbp2b
Ifit3b
Oas3
Isg15
Irf4
Dapk1
Gbp2
H2-M3
Ifit3
Oas2
Ddx58
Oasl1
Usp18
Xaf1
Irf7
Irf7 KO Fold Change
G
Irf7 downregulated baseline DEGs
Srsf7 downregulated baseline DEGs
480
26
73
Common baseline DEGs in Irf7 KO and Srsf7 KD
Psmb8
H2-Q6
Apol9b
H2-T24
Oas1g
Bst2
Gm38414
Oas1a
Phf11d
Ighm
Sdc3
H2-T23
Irf7
Isg15
Dhx58
Ifit3
Apol9a
Ifi204
Oasl1
Usp18
Ifi202b
Ifi27l2a
Rtp4
Gm29340
Ifi44l
Ifi44
Srsf7 KD#2
Irf7 KO #1

Figure S3: Supplemental data for Figure 3

A. Quantification of Figure 3E; n=2 **B.** Immunoblot of IRF7 and ACTIN protein levels over a time course of LPS stimulation (100 ng/ml) in WT iBMDMs. **C.** As in B but in WT BMDMs. **D.** Venn diagram depicting differential gene expression of *Irf7* KO1 at baseline vs. 4h +LPS (100ng/ml). Cut off: fold change < -1.5 and p-value <0.05. **E.** Top: BioPlanet Pathway Analysis of untreated *Irf7* KO gene expression. Bottom: BioPlanet Pathway Analysis of 4h +LPS *Irf7* KO gene expression. **F.** Heatmap depicting *Irf7* KO baseline gene expression from BioPlanet pathway analysis categories: “Interferon alpha/beta signaling,” ”Interferon signaling,” and “Interferon-gamma signaling pathway.” Duplicate terms removed. **G.** Left: Venn diagram depicting differentially expressed genes (DEGs) in *Irf7* KO1 (compared to GFP gRNA) and *Srsf7* KD (compared to SCR) RAW MΦs at baseline. Right: Heatmap of 26 genes in common between *Irf7* KO1 and *Srsf7* KD at baseline. Data are expressed as a mean of three biological replicates with error bars depicting SEM unless otherwise noted. Statistical significance was determined using two tailed unpaired student’s t test.

298 RAW MΦs at every time-point queried (**Fig. 3I**). IRF7 protein levels were lower in *Srsf7* knock-
299 down RAW MΦs at 0 and 4h but appeared to rebound at later time points (8 and 12h post-LPS)
300 (**Fig. 3J**), consistent with earlier data suggesting that IRF7 protein can be stabilization during
301 the innate response to infection (Ning et al., 2011). We also measured significantly less *Irf7*
302 transcript in *Srsf7* knockdown RAW MΦs in response to *M. tuberculosis* (**Fig. 3K**) and VSV in-
303 fection (**Fig. 3L**). Although we were only able to achieve modest knockdown of SRSF7 in
304 BMDMs transfected with an siRNA directed against *Srsf7* (alongside a non-targeting control;
305 siNC) (**Fig. 3M**), we can detect less IRF7 protein (**Fig. 3M**) and transcript (**Fig. 3N**) in these pri-
306 mary MΦs as well. Together, our data demonstrate a previously unappreciated role for SRSF7
307 in controlling *Irf7* transcript and protein levels in macrophage cell lines, primary macrophages,
308 (**Fig. 3I-J** and **3M-N**) and MEFs (**Fig. 2P**).
309
310 **IRF7 controls basal and induced expression of ISGs in RAW MΦs**
311 Our findings argue that loss of ISG expression in *Srsf7* knockdown cells stems primarily
312 from dampened levels of IRF7. However, as most literature points to a role for IRF7 in activated
313 immune cells, we were initially cautious to attribute basal ISG phenotypes in *Srsf7* knockdown
314 MΦs to IRF7. To better understand how IRF7 controls type I IFN responses in resting and acti-
315 vated RAW MΦs, we generated *Irf7* KO RAW MΦs using CRISPR-Cas9 editing with a gRNA de-
316 signed to target *Irf7* exon 3, and negative control cells expressing a GFP-specific (non-targeting)
317 gRNA. Two clonally expanded *Irf7* KO cell lines and a GFP gRNA control cell line were se-
318 lected, and loss of IRF7 protein was confirmed by immunoblot (**Fig. 3O**). Total RNA from un-
319 treated *Irf7* KO #1 and control cell lines, as well as from cells stimulated with LPS for 4h (100
320 ng/ml) were sent for RNA-seq analysis. We measured differential expression of 896 transcripts
321 (fold-change < -1.5; $p<0.05$) in *Irf7* KO vs. control cells at baseline and 1575 genes were differ-
322 entially expressed in *Irf7* KO MΦs at 4h post-LPS treatment (**Supplemental Table 3** and **Fig.**
323 **S3D**). Pathway analysis (BioPlanet Pathway Enrichment Analysis, NCATS (Huang et al., 2019))
324 identified a number of type I interferon-related pathways enriched for differentially expressed
325 genes in *Irf7* KO cells at baseline and at 4h post-LPS treatment (**Fig. S3E**). Consistent with our
326 hypothesis that SRSF7 controls ISG expression in an IRF7-dependent fashion, we found that
327 ISG expression was dramatically dampened in *Irf7* KO RAW MΦs at rest and after LPS stimula-
328 tion (**Figs. 3P-Q, S3F,** and **Supplemental Table 3**) and that differentially expressed ISGs were
329 largely shared between *Srsf7* KD and *Irf7* KO cells (**Fig. S3G**). Together, these data provide
330 strong evidence for IRF7 maintaining homeostatic expression of type I IFN and ISGs in macro-
331 phages and suggest that SRSF7 contributes to this circuit by mediating IRF7 expression.

332

333 **SRSF7 overexpression is sufficient to drive IRF7 and ISG expression**

334 We hypothesized that if SRSF7 can directly activate *Irf7* transcription, then overexpres-
335 sion of SRSF7 should be sufficient to drive *Irf7* expression. To test this model, we generated
336 doxycycline-inducible RAW MΦ cell lines that express 3xFLAG-SRSF7 or 3xFLAG-GFP. To en-
337 sure comparable levels of 3xFLAG-GFP and 3xFLAG-SRSF7 protein expression and to best
338 mimic endogenous levels of SRSF7, we tested and optimized treatment times, deciding on 2h
339 +DOX for 3xFLAG-GFP and 22h +DOX for 3xFLAG-SRSF7 (**Fig. 4A**). Notably, we found that
340 expression of SRSF7 alone was sufficient to increase the abundance of *Irf7* transcript (**Fig. 4B**),
341 IRF7 protein levels (**Fig. 4C**), and ISG transcripts (**Fig. 4D**) in otherwise unstimulated RAW
342 MΦs. Doxycycline-inducible expression of 3xFLAG-SRSF7 was also sufficient to drive expres-
343 sion of additional genes in the IRF7 baseline transcriptional regulon (*Xaf*, *Irak2*, *Ccl2*, and *Isg20*
344 (**Figs. 4E and S3G**)), lending further support to our hypothesis that SRSF7 controls ISG expres-
345 sion at the level of IRF7. We observed a similar phenotype in RAW MΦ cell lines that stably ex-
346 press 3xFLAG-SRSF7 compared to 3xFLAG-GFP controls (**Fig. 4F**). While overexpression of
347 3xFLAG-SRSF7 had a less pronounced impact on IRF7 transcript and protein expression after
348 LPS stimulation (**Fig. S4A-B)**, we measured a dramatic increase in *Irf7* and *Ifit3* transcript levels
349 in 3xFLAG-SRSF7-expressing stable cells upon infection with *M. tuberculosis* (**Fig. 4G**). Be-
350 cause expression of interferon stimulated genes has been associated with cell-intrinsic antibac-
351 terial control mechanisms and cell death pathways that impact bacterial spread (Banks et al.,
352 2019; Hoffpauir et al., 2020; MacMicking et al., 1997; MacMicking et al., 2003), we also asked
353 whether overexpression of SRSF7 affected *M. tuberculosis* replication. Briefly, we infected cells
354 with Mtb *luxBCADE* and followed bacterial replication as a measure of relative light units (as in
355 (Bell et al., 2021; Wagner et al., 2022)). We measured a significant increase in RLUs at Day 3
356 post-infection (**Fig. 4H**) suggesting that SRSF7 expression may help control *M. tuberculosis*
357 replication and/or spread. Together, these data suggest a direct role for SRSF7 in activating ex-
358 pression of *Irf7* and promoting type I interferon responses in MΦs.

359

360 **SRSF7 promotes STAT1 association and RNAPII elongation at the *Irf7* promoter**

361 Having established that decreased levels of IRF7 is the likely culprit for the type I IFN
362 defect in *Srsf7* knockdown MΦs (**Fig. 3**) and demonstrated that SRSF7 overexpression is suffi-
363 cient to promote *Irf7* expression (**Fig. 4**), we set out to determine the mechanism though which
364 SRSF7 controls *Irf7* expression. Earlier work has implicated SR proteins in coupling transcrip-
365 tion and splicing and have been shown to influence transcription by interacting with histone tails

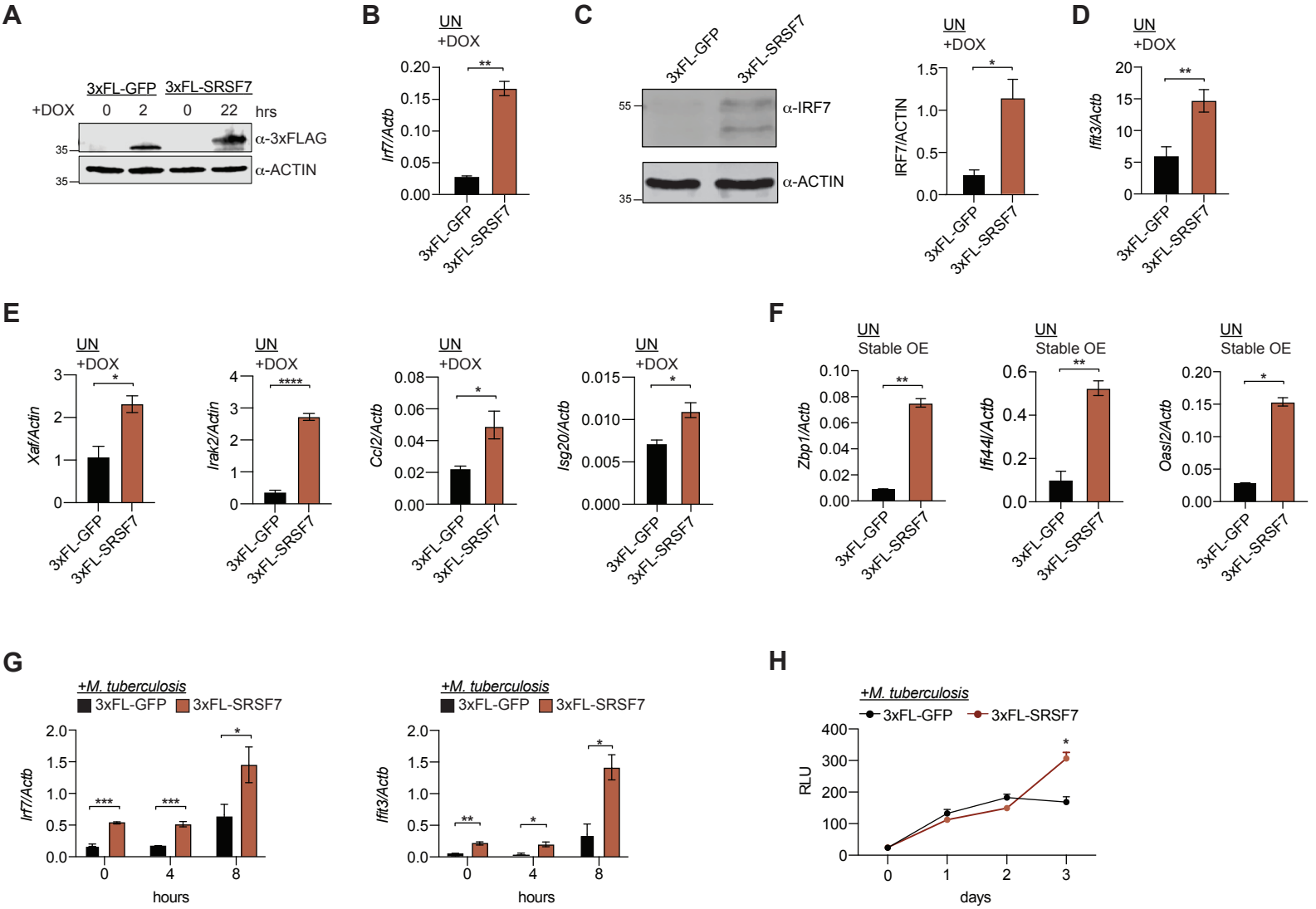
A
3xFL-GFP
3xFL-SRSF7
+DOX
0
2
0
22
hrs
35
α-3xFLAG
35
α-ACTIN
B
UN
+DOX
Irf7/Actb
0.20
0.15
0.10
0.05
0.00
**
3xFL-GFP
3xFL-SRSF7
C
3xFL-GFP
3xFL-SRSF7
55
α-IRF7
35
α-ACTIN
UN
+DOX
IRF7/ACTIN
1.5
1.0
0.5
0.0
*
3xFL-GFP
3xFL-SRSF7
D
UN
+DOX
Ifit3/Actb
20
15
10
5
0
**
3xFL-GFP
3xFL-SRSF7
E
UN
+DOX
Xaf/Actin
3
2
1
0
*
3xFL-GFP
3xFL-SRSF7
UN
+DOX
Irak2/Actin
4
3
2
1
0
****
3xFL-GFP
3xFL-SRSF7
UN
+DOX
Ccl2/Actb
0.08
0.06
0.04
0.02
0.00
*
3xFL-GFP
3xFL-SRSF7
UN
+DOX
Isg20/Actb
0.015
0.010
0.005
0.000
*
3xFL-GFP
3xFL-SRSF7
F
UN
Stable OE
Zbp1/Actb
0.10
0.08
0.06
0.04
0.02
0.00
**
3xFL-GFP
3xFL-SRSF7
UN
Stable OE
Ifi44l/Actb
0.6
0.4
0.2
0.0
**
3xFL-GFP
3xFL-SRSF7
UN
Stable OE
Oasl2/Actb
0.20
0.15
0.10
0.05
0.00
*
3xFL-GFP
3xFL-SRSF7
G
+M. tuberculosis
3xFL-GFP
3xFL-SRSF7
Irf7/Actb
2.0
1.5
1.0
0.5
0.0
***
***
*
0
4
8
hours
+M. tuberculosis
3xFL-GFP
3xFL-SRSF7
Ifit3/Actb
2.0
1.5
1.0
0.5
0.0
**
*
*
0
4
8
hours
H
+M. tuberculosis
3xFL-GFP
3xFL-SRSF7
RLU
400
300
200
100
0
*
0
1
2
3
days

Figure 4

759 **Figure 4: SRSF7 overexpression is sufficient to drive basal expression of IRF7 and ISGs**
760
761 **A.** Immunoblot of 3xFLAG-GFP or 3xFLAG-SRSF7 tetracycline inducible RAW MΦs treated with
762 doxycycline (DOX) (1 µg/ml). 3xFLAG-GFP MΦs received DOX for 2h and 3xFLAG-SRSF7 MΦs
763 received DOX for 22h. ACTIN shown as loading control. **B.** RT-qPCR of *Irf7* in 3xFLAG-GFP (2h
764 DOX treatment) and 3xFLAG-SRSF7 (22h DOX treatment) inducible RAW MΦs at baseline. **C.**
765 Immunoblot of IRF7 in 3xFLAG-GFP (2h DOX treatment) and 3xFLAG-SRSF7 (22h dox treat-
766 ment) inducible RAW MΦs at baseline. Quantification right. **D.** As in B but for *Ifit3*. **E.** As in B but
767 for *Xaf, Irak2, Ccl2,* and *Isg20*. **F.** RT-qPCR of *Zbp1*, *Ifi44*, or *Oasl2* in 3xFLAG-GFP and 3xFLAG-
768 SRSF7 stable overexpression RAW MΦs at baseline. **G.** RT-qPCR of *Irf7* or *Ifit3* at 0, 4, and 8h
769 post-infection with Mtb (Erdman; MOI=5). **H.** Mtb *luxBCADE* replication in 3xFLAG-GFP and
770 3xFL-SRSF7 doxycycline-inducible RAW MΦs measured by relative light units (RLUs) over time
771 course (Erdman; MOI=1). Data are expressed as a mean of three biological replicates with error
772 bars depicting SEM. Statistical significance was determined using two tailed unpaired student's t
773 test. *=p<0.05, **=p<0.01, ***=p<0.001.
774
775
776
777
778
779
780
781
782
783
784
785
786
787
788
789
790
791
792

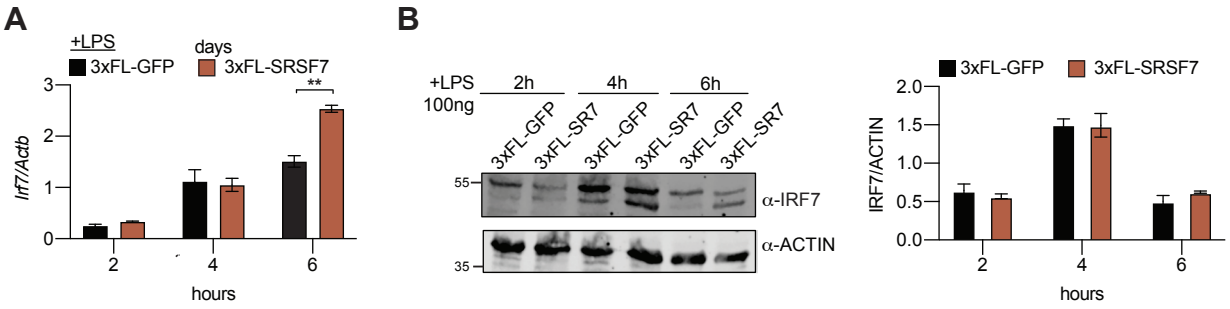
A
+LPS
days
3xFL-GFP
3xFL-SRSF7
**
Irf7/Actb
3
2
1
0
2
4
6
hours
B
+LPS
100ng
2h
4h
6h
3xFL-GFP
3xFL-SR7
3xFL-GFP
3xFL-SR7
3xFL-GFP
3xFL-SR7
55
35
α-IRF7
α-ACTIN
3xFL-GFP
3xFL-SRSF7
IRF7/ACTIN
2.0
1.5
1.0
0.5
0.0
2
4
6
hours

Figure S4: Supplemental data for Figure 4

A. RT-qPCR of *Irf7* in 3xFLAG-GFP (2h dox treatment) and 3xFLAG-SRSF7 (22h dox treatment) inducible RAW MΦs over a time course of LPS stimulation (100 ng/ml). **B.** Immunoblot of IRF7 in 3xFLAG-GFP (2h dox treatment) and 3xFLAG-SRSF7 (22h dox treatment) inducible RAW MΦs over a time course of LPS stimulation (100 ng/ml) (quantification right). Data are expressed as a mean of three biological replicates with error bars depicting SEM. Statistical significance was determined using two tailed unpaired student's t test. *=$p<0.05$, **=$p<0.01$, ***=$p<0.001$.

366 (Loomis et al., 2009; Luco et al., 2011; Luco et al., 2010) or by directly mediating transcriptional
367 elongation via pTEFb (Ji et al., 2013). To begin to investigate a role for SRSF7 in activating *Irf7*
368 transcription, we performed chromatin immunoprecipitation (ChIP)-qPCR for RNA polymerase II
369 (RNAPII) in *Srsf7* knockdown and SCR control MΦs at 4h post-LPS treatment, using primers de-
370 signed to tile the *Irf7* promoter region (100bp amplicon, 100 bp apart from each other (**Fig. 5A**))
371 and an antibody that recognizes both phosphorylated and unphosphorylated forms of the C-ter-
372 minal domain of the largest subunit of RNAPII. We observed dramatic accumulation of RNAPII
373 at/around the *Irf7* transcription start site (TSS) (-400 to +250) in *Srsf7* knockdown MΦs (**Fig. 5B**,
374 teal). This pattern of RNAPII in *Srsf7* knockdown MΦs is suggestive of a pile-up resulting from a
375 failure to convert to a successful elongation complex. We next asked whether a defect in
376 RNAPII clearance could be explained by defects in recruitment or retention of transcription fac-
377 tors like STAT1 to the *Irf7* promoter. Using ChIP-qPCR with an antibody against Y701 STAT1,
378 we measured a near total loss of STAT1 signal in *Srsf7* knockdown MΦs (**Fig. 5C**). An analo-
379 gous set of ChIP-qPCRs at the promoter of *Ifit3*, another ISG whose expression is SRSF7-de-
380 pendent, showed no differences in RNAPII or STAT1 occupancy in *Srsf7* knockdown cells
381 (**Figs. 5D-F**). Likewise, we saw no difference in RNAPII occupancy in *Srsf7* knockdown MΦs at
382 the promoter of *Stat1* itself (**Figs. 5G-H**). Consistent with upregulation of *Irf7* transcript and pro-
383 tein levels (**Figs. 4B-C**), overexpression of 3xFLAG-SRSF7 was sufficient to recruit significant
384 levels of STAT1 to the *Irf7* promoter in resting macrophages (**Fig. 5I**). These data support a
385 role for SRSF7 in promoting transcription of *Irf7* and suggest that dampened expression of ISGs
386 like *Ifit3* in *Srsf7* knockdown MΦs occurs indirectly, downstream of *Irf7* transcriptional defects.
387 Having linked STAT1 binding and RNAPII elongation at the *Irf7* promoter to SRSF7, we
388 next asked whether SRSF7 carries out this function by directly associating with the *Irf7* genomic
389 locus. Lacking ChIP-grade antibodies for SRSF7, we turned back to our doxycycline-inducible
390 3xFLAG-SRSF7 and 3xFLAG-GFP cell lines (**Fig. 4A**) and performed anti-FLAG ChIP-qPCR at
391 the *Irf7* promoter using the same primer sets shown in Fig. 6A. Consistent with a direct role for
392 SRSF7 in facilitating STAT1 recruitment and RNAPII elongation at *Irf7*, we observed significant
393 enrichment of 3xFLAG-SRSF7 at the *Irf7* promoter (-500 to 0) in both resting (**Fig. 5J**) and LPS-
394 treated macrophages (4h post-LPS) (**Fig. 5K**) with no SRSF7 enrichment at *Ifit3* (**Fig. 5L**). To
395 determine the extent to which SRSF7 globally associates with promoter regions, we performed
396 ChIP-seq. Briefly, reads were trimmed by Cutadapt and aligned to the *Mus musculus* genome
397 build mm10 using Bowtie. After quality control, peaks were called using MACS2 with input/IgG
398 controls background subtracted. We detected 548 unique peaks for SRSF7 across the genome,
399 with approximately half of these peaks detected at transcription start sites (**Figs. 5M and S5A-**

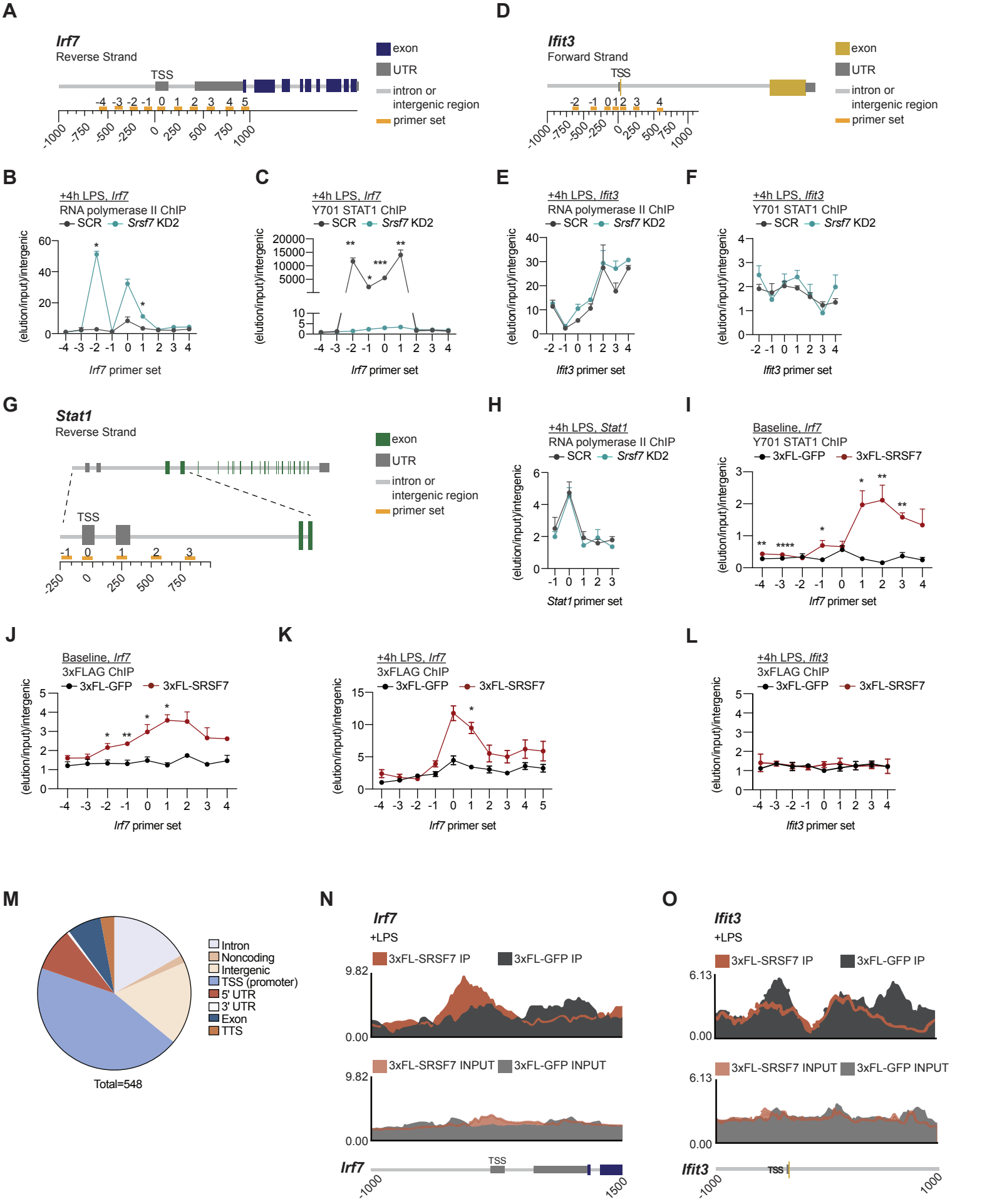
A
Irf7
Reverse Strand
TSS
exon
UTR
intron or intergenic region
primer set
D
Ifit3
Forward Strand
TSS
B
+4h LPS, Irf7
RNA polymerase II ChIP
SCR
Srsf7 KD2
(elution/input)/intergenic
Irf7 primer set
C
+4h LPS, Irf7
Y701 STAT1 ChIP
E
+4h LPS, Ifit3
RNA polymerase II ChIP
Ifit3 primer set
F
+4h LPS, Ifit3
Y701 STAT1 ChIP
G
Stat1
Reverse Strand
H
+4h LPS, Stat1
RNA polymerase II ChIP
Stat1 primer set
I
Baseline, Irf7
Y701 STAT1 ChIP
3xFL-GFP
3xFL-SRSF7
J
Baseline, Irf7
3xFLAG ChIP
K
+4h LPS, Irf7
3xFLAG ChIP
L
+4h LPS, Ifit3
3xFLAG ChIP
M
Intron
Noncoding
Intergenic
TSS (promoter)
5' UTR
3' UTR
Exon
TTS
Total=548
N
Irf7
+LPS
3xFL-SRSF7 IP
3xFL-GFP IP
3xFL-SRSF7 INPUT
3xFL-GFP INPUT
O
Ifit3
+LPS

Figure 5

827 **Figure 5: SRSF7 recruitment to the *Irf7* promoter maximizes STAT1 association and pro-**
828 **motes RNA polymerase II elongation**
829
830 **A.** Diagram of the *Irf7* gene with tiling primers designed around the transcriptional start site (or-
831 ange). **B.** RNA polymerase II ChIP-qPCR (antibody recognizes both modified and unmodified
832 CTD) at the *Irf7* promoter in SCR and *Srsf7* KD RAW MΦs 4h post-LPS stimulation (100ng/ml).
833 Data represented as elution/input normalized to that of an intergenic control primer set. **C.** Y701
834 STAT1 ChIP-qPCR at the *Irf7* promoter in SCR or *Srsf7* KD RAW MΦs 4h post-LPS stimulation
835 (100 ng/ml). Data represented as elution/input normalized to that of an intergenic control. **D.** Dia-
836 gram of the *Ifit3* gene with tiling primers designed around the transcriptional start site (orange). **E.**
837 As in B but at the *Ifit3* promoter. **F.** As in C but at the *Ifit3* promoter. **G.** Diagram of the *Stat1* gene
838 with tiling primers designed around the transcriptional start site (orange). **H.** As in B but at the
839 *Stat1* promoter. **I.** Y701 STAT1 ChIP-qPCR at the *Irf7* promoter in 3xFLAG-GFP and 3xFLAG-
840 SRSF7 dox-inducible RAW MΦs at baseline. **J.** 3xFLAG ChIP-qPCR of 3xFLAG-GFP and
841 3xFLAG-SRSF7 in dox-inducible RAW MΦs at baseline. **K.** 3xFLAG ChIP-qPCR of 3xFLAG-GFP
842 and 3xFLAG-SRSF7 in dox-inducible RAW MΦs at the *Irf7* promoter 4h post LPS stimulation (100
843 ng/ml). **L.** As in K at the *Ifit3* promoter. **M.** Categorization of unique 3xFLAG ChIP peaks in 3xFL-
844 SRSF7 dox-inducible RAW MΦs 4h post-LPS (100 ng/ml). **N.** Enrichment of 3xFLAG-SRSF7 and
845 3xFLAG-GFP at the *Irf7* promoter by ChIP-seq: IP (top) and input (bottom). **O.** As in M but at the
846 *Ifit3* promoter. Unless otherwise noted, data are expressed as a mean of three or more biological
847 replicates with error bars depicting SEM. ChIP-qPCRs are shown as the mean of three or more
848 technical replicates with error bars depicting SEM. Statistical significance was determined using
849 two tailed unpaired student's t test. *=p<0.05, **=p<0.01, ***=p<0.001.
850
851
852
853
854
855
856
857
858
859
860

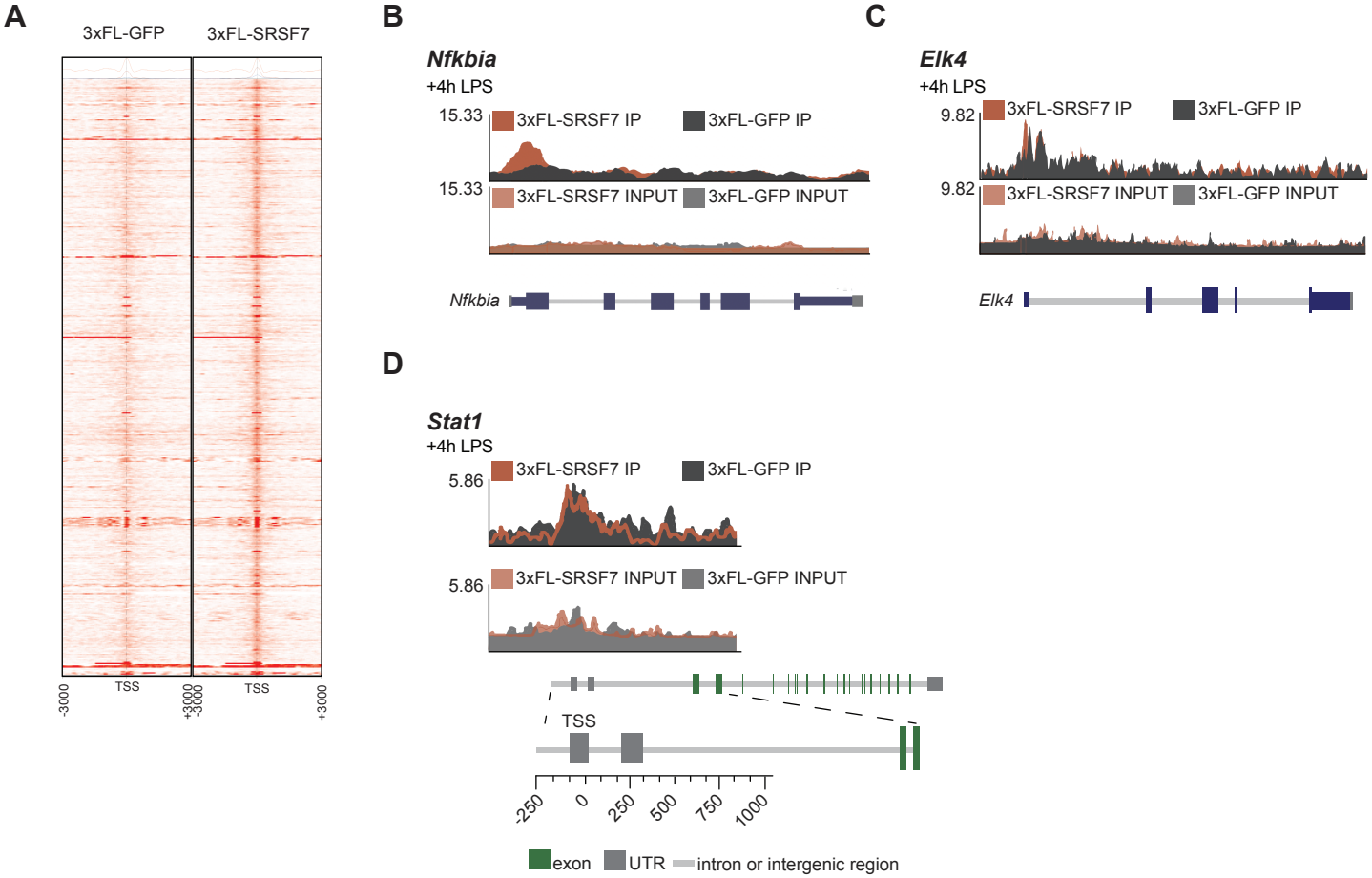

E

Motif

Name	P-value	Percent of Targets	Percent of Background
Etv2(ETS)/ES-ER71-ChIP-Seq(GSE59402)/Homer	1e-6	16.79%	9.68%
ZNF41(Zf)/HEK293-ZNF41.GFP-ChIP-Seq(GSE58341)/Homer	1e-6	1.46%	0.11%
Fli1(ETS)/CD8-FLI-ChIP-Seq(GSE20898)/Homer	1e-6	25.36%	17.02%
AT1G76870(Trihelix)/col-AT1G76870-DAP-Seq(GSE60143)/Homer	1e-6	4.93%	1.63%
Elk4(ETS)/Hela-Elk4-ChIP-Seq(GSE31477)/Homer	1e-5	19.34%	12.62%
ETV4(ETS)/HepG2-ETV4-ChIP-Seq(ENCODE)/Homer	1e-4	25.36%	18.08%
ETS(ETS)/Promoter/Homer	1e-4	12.04%	7.09%
ELF1(ETS)/Jurkat-ELF1-ChIP-Seq(SRA014231)/Homer	1e-4	17.34%	11.50%
NAM(NAC)/col-NAM-DAP-Seq(GSE60143)/Homer	1e-4	16.06%	10.71%

Figure S5: Supplemental data for Figure 5

A. Heatmap indicating read coverage density at transcriptional start sites (TSS) in 3xFL-GFP or 3xFL-SRSF7 dox-inducible RAW MΦs, 4h post-LPS treatment. **B.** Enrichment of 3xFLAG-SRSF7 and 3xFLAG-GFP at the *Nfkbia* promoter by ChIP-seq: IP (top) and input (bottom). **C.** Enrichment of 3xFLAG-SRSF7 and 3xFLAG-GFP at the *Elk4* promoter by ChIP-seq: IP (top) and input (bottom). **D.** Enrichment of 3xFLAG-SRSF7 and 3xFLAG-GFP at the *Stat1* promoter by ChIP-seq: IP (top) and input (bottom). **E.** Putative SRSF7 motifs predicted by HOMER from 3xFLAG-SRSF7 ChIP-seq data.

400 **C**). By ChIP-seq we again saw clear enrichment of 3xFLAG-SRSF7 at the *Irf7* promoter (**Fig. 5N**),
401 but not at *Ifit3* (**Fig. 5O**) or *Stat1* (**Fig. S5D**). Although SRSF7 peaks were called at several im-
402 mune associated genes, including *Fos*, *Myd88*, *Ifitm3*, and *Dusp5*, there was no evidence for
403 SRSF7 enrichment at the promoter of any other type I IFN response-associated transcription fac-
404 tors (**Supplemental Table 4**). Taken together, our ChIP-seq data argue against universal asso-
405 ciation of SRSF7 with gene promoters, as was reported for factors like SRSF1 and SRSF2 (Ji et
406 al., 2013), and instead support a privileged role for SRSF7 in facilitating transcription at specific
407 genes like *Irf7*.
408
409 **SRSF7 interacts with the H4K20me1 histone methyltransferase KMT5a/SET8 to promote**
410 ***Irf7* transcription**
411 ChIP-seq did not reveal a strong consensus sequence for SRSF7 and even weak consen-
412 sus sequence enrichment was only detected at subsets of genes (**Fig. S5E**). As this argues
413 against recruitment of SRSF7 to the *Irf7* promoter via a specific DNA-encoded motif, we hypoth-
414 esized that SRSF7 could be brought to/retained at the *Irf7* promoter via one or more protein-
415 protein interactions. To begin to explore this possibility, we generated RAW MΦ cell lines stably
416 expressing 3xFLAG-SRSF1, 3xFLAG-SRSF3, 3xFLAG-SRSF6, 3xFLAG-SRSF9, in addition to
417 the previously described 3xFLAG-SRSF7 and 3xFLAG-GFP cell lines. We performed a series of
418 immunoprecipitation experiments followed by mass spectrometry to identify peptides enriched in
419 each pulldown. Although many protein binding partners were shared between SRSF7 and other
420 SR protein family members (e.g. SR proteins, hnRNPs, RRM domain-containing proteins) (**Fig.**
421 **S6A**), peptides derived from components of the KMT5a/SET8 histone methyltransferase complex
422 were unique to SRSF7 (**Fig. 6A**). KMT5a is the sole histone methyltransferase responsible for
423 depositing monomethylation at H4K20. H4K20me1 levels are linked to the cell cycle and during
424 mitosis H4K20me1 mediates chromatin condensation (van Nuland and Gozani, 2016). Several
425 studies report enrichment of H4K20me1 at actively transcribed genes (Barski et al., 2007),
426 (Veloso et al., 2014) and it has been implicated in facilitating RNAPII escape from promoter-prox-
427 imal regions (Nikolaou et al., 2017). We confirmed interaction between 3xFLAG-SRSF7 and
428 KMT5a in macrophages by immunoprecipitation/immunoblot, using antibodies against endoge-
429 nous KMT5a (**Fig. 6B**).
430 To determine a role for KMT5a in mediating *Irf7* expression, we silenced its expression
431 via siRNA transfection in RAW MΦs, alongside a non-targeting control. We found that loss of
432 KMT5a dampened *Irf7* transcript levels and those of downstream ISGs, phenocopying SRSF7
433 knockdown (**Fig. 6C**). Expression of inflammatory genes outside the *Irf7* regulon, like *Tnf*, was

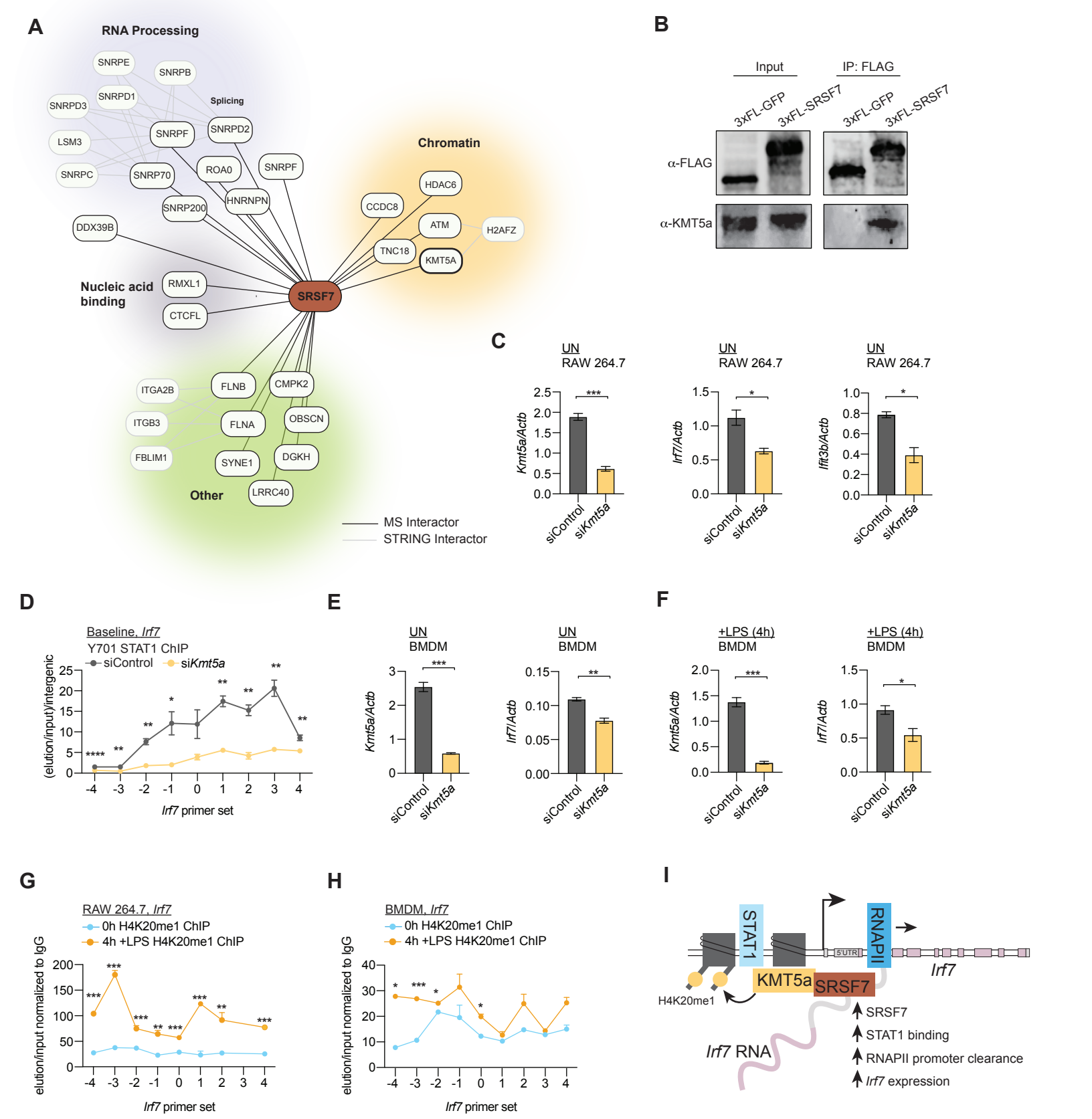
A
RNA Processing
Splicing
Chromatin
Nucleic acid binding
Other
SRSF7
MS Interactor
STRING Interactor
B
Input
IP: FLAG
3xFL-GFP
3xFL-SRSF7
α-FLAG
α-KMT5a
C
UN
RAW 264.7
Kmt5a/Actb
Irf7/Actb
Ifit3b/Actb
siControl
siKmt5a
D
Baseline, Irf7
Y701 STAT1 ChIP
siControl
siKmt5a
(elution/input)/intergenic
Irf7 primer set
E
UN
BMDM
F
+LPS (4h)
BMDM
G
RAW 264.7, Irf7
0h H4K20me1 ChIP
4h +LPS H4K20me1 ChIP
elution/input normalized to IgG
H
BMDM, Irf7
I
STAT1
RNAPII
5'UTR
Irf7
KMT5a
SRSF7
H4K20me1
Irf7 RNA
SRSF7
STAT1 binding
RNAPII promoter clearance
Irf7 expression

Figure 6

895 **Figure 6: SRSF7 interacts with the H4K20me1 histone methyltransferase KMT5a/SET8 to**
896 **promote *Irf7* transcription**
897
898 **A.** Proteins identified as unique interactors of 3xFL-SRSF7 in RAW MΦs at baseline by IP-LC/MS.
899 **B.** Immunoblot of immunoprecipitation of 3xFL-SRSF7 (+DOX 1 µg/ml 22h), 3xFL-GFP (+DOX 1
900 µg/ml 2h) and endogenous KMT5a/SET8. **C.** RT-qPCR of *Kmt5a, Irf7*, or *Ifit3b* in RAW MΦs trans-
901 fected with siControl or si*Kmt5a* siRNA at baseline. **D.** Y701 STAT1 ChIP-qPCR at the *Irf7* pro-
902 moter in siControl or si*Kmt5a/Set8* RAW MΦs at baseline. Data represented as elution/input nor-
903 malized to that of an intergenic control. **E.** RT-qPCR of *Kmt5a* and *Irf7* in bone marrow derived
904 macrophages (BMDMs) transfected with siControl or si*Kmt5a* siRNA. **F.** As in E but at 4h post-
905 stimulation with LPS (100 ng/ml). **G.** H4K20me1 ChIP-qPCR in RAW MΦs at baseline or 4h post
906 stimulation with 100 ng/ml LPS at the *Irf7* promoter. Data represented as elution/input normalized
907 to IgG. **H.** As in G but in BMDMs. **I.** Proposed model for cooperation between SRSF7 and KMT5a
908 promoting transcriptional activation of *Irf7*. Unless otherwise noted, data are expressed as a mean
909 of three or more biological replicates with error bars depicting SEM. ChIP-qPCRs are shown as
910 the mean of three or more technical replicates with error bars depicting SEM. Statistical signifi-
911 cance was determined using two tailed unpaired student's t test. *=$p<0.05$, **=$p<0.01$,
912 ***=$p<0.001$.
913
914
915
916
917
918
919
920
921
922
923
924
925
926
927
928

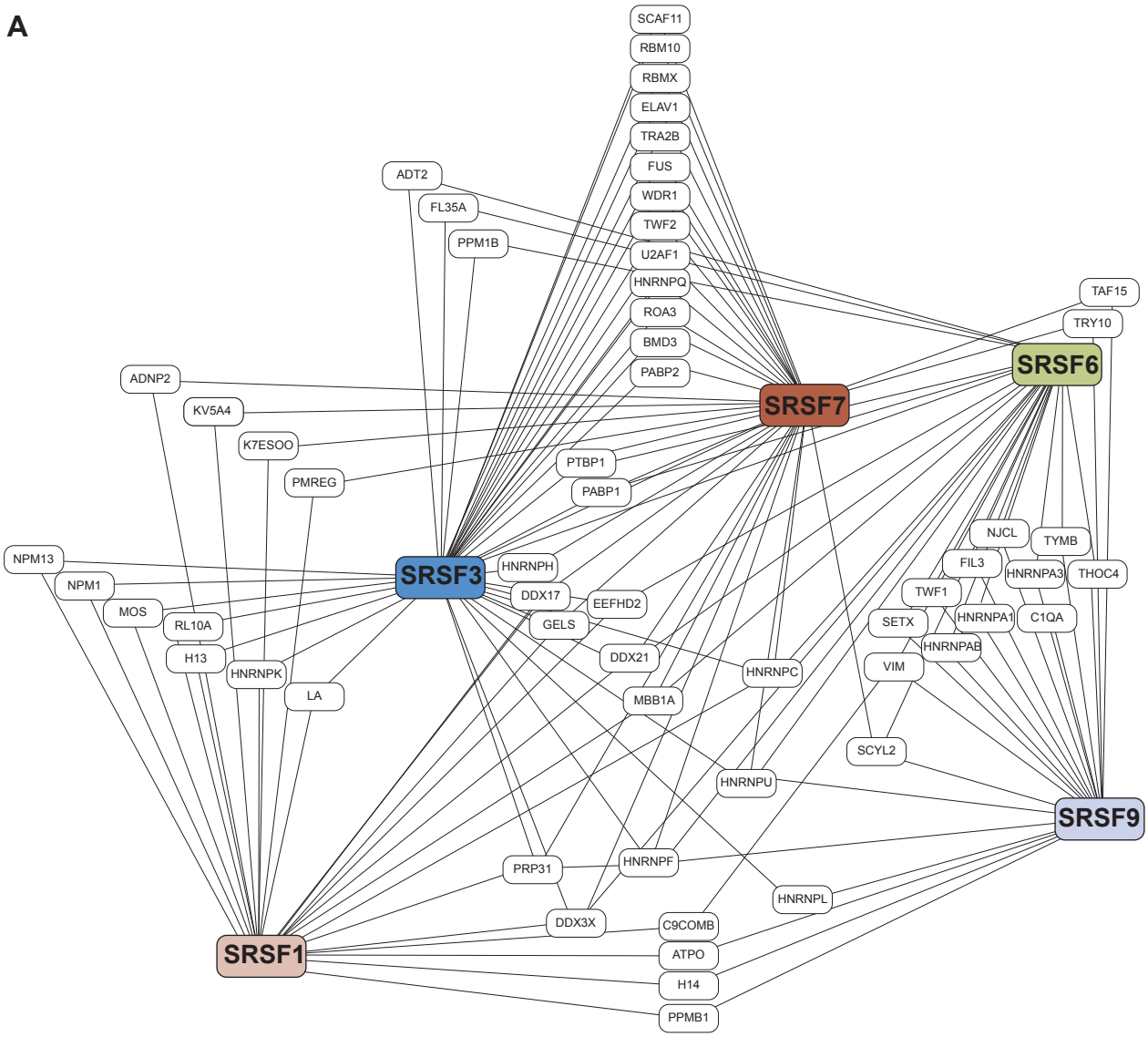
A
SCAF11
RBM10
RBMX
ELAV1
TRA2B
FUS
WDR1
TWF2
U2AF1
HNRNPQ
ROA3
BMD3
PABP2
ADT2
FL35A
PPM1B
TAF15
TRY10
SRSF6
SRSF7
ADNP2
KV5A4
K7ESOO
PMREG
PTBP1
PABP1
NPM13
NPM1
MOS
RL10A
H13
HNRNPK
LA
SRSF3
HNRNPH
DDX17
EEFHD2
GELS
DDX21
MBB1A
HNRNPC
NJCL
TYMB
FIL3
HNRNPA3
THOC4
TWF1
SETX
HNRNPA1
C1QA
HNRNPAB
VIM
SCYL2
HNRNPU
SRSF9
PRP31
HNRNPF
HNRNPL
DDX3X
C9COMB
ATPO
H14
PPMB1
SRSF1

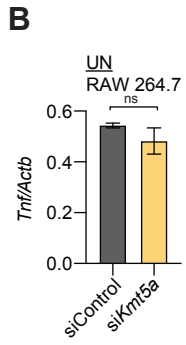
B
UN
RAW 264.7
ns
Tnf/Actb
0.6
0.4
0.2
0.0
siControl
siKmt5a

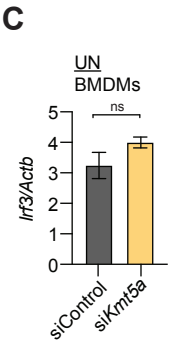
C
UN
BMDMs
ns
Irf3/Actb
5
4
3
2
1
0
siControl
siKmt5a

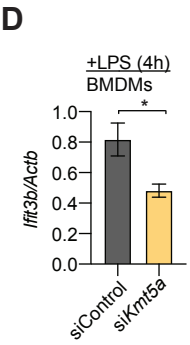
D
+LPS (4h)
BMDMs
*
Ifit3b/Actb
1.0
0.8
0.6
0.4
0.2
0.0
siControl
siKmt5a

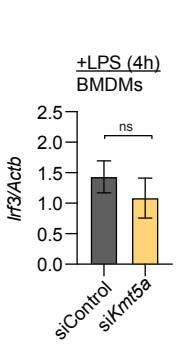
+LPS (4h)
BMDMs
ns
Irf3/Actb
2.5
2.0
1.5
1.0
0.5
0.0
siControl
siKmt5a

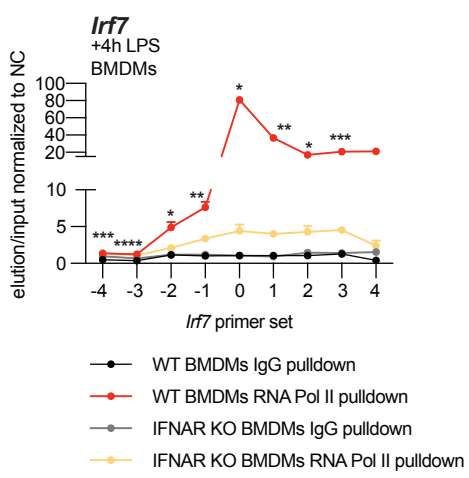
E
Irf7
+4h LPS
BMDMs
elution/input normalized to NC
100
80
60
40
20
10
5
0
-4
-3
-2
-1
0
1
2
3
4
Irf7 primer set
WT BMDMs IgG pulldown
WT BMDMs RNA Pol II pulldown
IFNAR KO BMDMs IgG pulldown
IFNAR KO BMDMs RNA Pol II pulldown

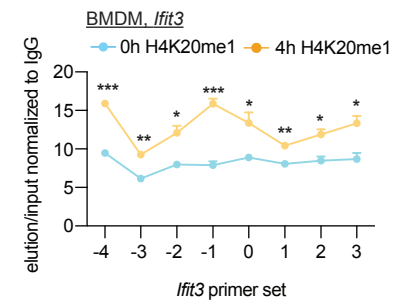
F
BMDM, Ifit3
0h H4K20me1
4h H4K20me1
elution/input normalized to IgG
20
15
10
5
0
-4
-3
-2
-1
0
1
2
3
Ifit3 primer set

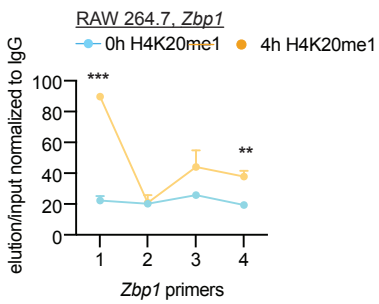
G
RAW 264.7, Zbp1
0h H4K20me1
4h H4K20me1
elution/input normalized to IgG
100
80
60
40
20
0
1
2
3
4
Zbp1 primers

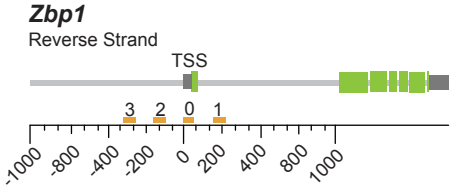
Zbp1
Reverse Strand
TSS
3
2
0
1
-1000
-800
-400
-200
0
200
400
800
1000

929 **Figure S6: Supplemental data for Figure 6**

930

931 **A.** Proteins identified as shared interactors of 3xFL-SRSF7, 3xFL-SRSF1, 3xFL-SRSF3, 3xFL-
932 SRSF6, and 3xFL-SRSF9 in RAW MΦs at baseline by IP-LC/MS. **B.** RT-qPCR of *Tnf* in RAW
933 MΦs transfected with siControl or si*Kmt5a* siRNA at baseline. **C.** RT-qPCR of *Irf3* in BMDMs
934 transfected with siControl or si*Kmt5a* siRNA at baseline. **D.** As in C but 4h post-stimulation with
935 100 ng/ml LPS. **E.** RNA polymerase II ChIP-qPCR 4h post-stimulation with LPS in WT and *Ifnar*
936 -/- BMDMs at the *Irf7* promoter **F.** H4K20me1 ChIP-qPCR at the *Ifit3* promoter in RAW MΦs at
937 baseline or 4h post- stimulation with 100 ng/ml LPS. **G.** As in F at the *Zbp1* promoter. Right:
938 Diagram of the *Zbp1* gene with tiling primers designed around the transcriptional start site (or-
939 ange). Unless otherwise noted, data are expressed as a mean of three or more biological repli-
940 cates with error bars depicting SEM. ChIP-qPCRs are shown as the mean of three or more tech-
941 nical replicates with error bars depicting SEM. Statistical significance was determined using two
942 tailed unpaired student's t test. *=p<0.05, **=p<0.01, ***=p<0.001.

943
944
945
946
947
948
949
950
951
952
953
954
955
956
957
958
959
960
961
962

434 not impacted by loss of KMT5a (**Fig. S6B**), hinting at a privileged role for KMT5a in modulating
435 ISGs. Notably, STAT1 failed to associate with the *Irf7* promoter in *Kmt5a* knockdown RAW MΦs
436 (**Fig. 6D**), strongly supporting a role for KMT5a in promoting a pro-transcription chromatin envi-
437 ronment at *Irf7*. We also detected lower *Irf7* transcript levels both at rest (**Fig. 6E**) and at 4h post-
438 LPS treatment (**Fig. 6F**) when we knocked down KMT5a in BMDMs. Together, these data impli-
439 cate KMT5a in stimulating *Irf7* expression in macrophages.

440 Lastly, we sought to implicate the histone mark deposited by KMT5a, H4K20me1, in acti-
441 vating *Irf7* expression. We found that LPS treatment triggered significant accumulation of
442 H4K20me1 at the *Irf7* promoter in both RAW MΦs (**Fig. 6G**) and BMDMs (**Fig. 6H**) that was
443 concomitant with IFNAR-dependent transcriptional activation and recruitment of RNAPII (**Fig.
444 S6E**). LPS treatment also elevated H4K20me1 levels at ISGs like *Ifit3* and *Zbp1* (**Fig. S6F-G**).
445 Because we did not see SRSF7 enrichment at the promoters of these or other ISGs by ChIP-
446 qPCR or ChIP-seq (**Fig. 5L**), our data argue that H4K20me1 does not recruit SRSF7 to promot-
447 ers. Instead, our data support a model wherein interaction between SRSF7 and KMT5a confers
448 tight control over the chromatin landscape at *Irf7* promoter, which is required to maximize STAT1
449 recruitment and promote RNAPII elongation (**Fig. 6I**).
450

451 **DISCUSSION**

452 Because of their potential to activate large gene regulons, cells need to exert tight con-
453 trol over transcription factors themselves. This is particularly true for transcription factors that
454 activate inflammatory immune gene expression, which are subject to multiple layers of post-
455 translational regulation (cytoplasmic sequestration, phosphorylation, proteasomal degradation)
456 (Caamano and Hunter, 2002; Jefferies, 2019; Ning et al., 2011; Smale, 2012). Here, we de-
457 scribe a novel role for the splicing regulatory protein SRSF7 in stimulating the type I IFN re-
458 sponse by activating transcription of the *Irf7* gene. We demonstrate that enrichment of SRSF7
459 at the *Irf7* promoter facilitates association of the transcription factor STAT1 and promotes
460 RNAPII elongation and initiate expression of *Irf7*. SRSF7 accomplishes this by establishing a
461 pro-transcription chromatin landscape at the *Irf7* promoter via interaction with the H4K20me1
462 methyltransferase KMT5a. By controlling IRF7 abundance, SRSF7 plays a privileged role in reg-
463 ulating both antiviral (**Fig. 2Q-T**) and antibacterial (**Fig. 5H**) innate immune responses in macro-
464 phages. In addition to implicating SRSF7 in activating *Irf7* expression, this work highlights a criti-
465 cal and underappreciated role for both SRSF7 and IRF7 in maintaining tonic and early interferon
466 signaling in MΦs.

467 A major finding of this study relates to the ability of SRSF7—a canonical RNA binding
468 protein—to promote transcription of *Irf7*. Over the past two decades, the idea that transcription
469 and RNA processing occur in a linear, stepwise fashion has been repeatedly challenged. It is
470 now generally accepted that many steps in RNA processing (i.e. capping, pre-mRNA splicing,
471 RNA editing) occur co-transcriptionally while nascent transcripts are still bound to RNAPII. Ac-
472 cordingly, splicing can influence transcription and transcription can impact splicing (Tellier et al.,
473 2020). Several studies have linked SR proteins to RNAPII dynamics and co-transcriptional
474 splicing. SRSF2, for example, releases the cyclin-dependent kinase pTEFb from an inhibitory
475 7SK-containing complex to relieve stalled polymerase at promoters (Ji et al., 2013) and SRSF3
476 regulates exon inclusion via the C-terminal domain of RNAPII (de la Mata and Kornblihtt, 2006).
477 Although our data suggest an analogous role for SRSF7 in mediating transcription factor binding
478 and RNAPII elongation at the *Irf7* promoter, several aspects of this mechanism still need to be
479 explored.
480 One outstanding question relates to why we see SRSF7 at certain promoters, like *Irf7*,
481 but not others (**Fig. 6**). Owing to its ability to interact with histone modifying enzymes like
482 KMT5a, it is possible that the local chromatin environment dictates the specificity of SRSF7 pro-
483 moter enrichment. Our data demonstrate that H4K20me1 levels are significantly enhanced at
484 the promoters of innate genes including *Irf7* following LPS treatment, linking this mark to macro-
485 phage activation and innate immune responses for the first time. However, because H4K20me1
486 is enriched at innate genes like *Ifit3* and *Zbp1* where SRSF7 promoter association was not de-
487 tected (**Fig. S6F-G**), we currently do not favor a "chromatin recruits SRSF7" model. Instead, we
488 propose that specificity is dictated by sequences encoded in exons/introns of genes down-
489 stream of SRSF7-sensitive promoters, such that nascent RNAs serve as the platform for SRSF7
490 recruitment. The reported consensus sequence for SRSF7 is GA(C/T)GA(C/T) (Cavaloc et al.,
491 1999) and SRSF7 was shown to bind TGA(C/T)C sequences in its own pre-mRNA to regulate
492 poison cassette exon inclusion (Konigs et al., 2020). We can detect several potential SRSF7
493 bindings sites in the first coding exon of *Irf7* (TGACC). Thus, it is possible that SRSF7's associ-
494 ation at the *Irf7* promoter occurs by virtue of co-transcriptional binding of exonic splicing enhanc-
495 ers (ESEs) in nascent transcripts.
496 It is also conceivable that SRSF7 associates with the *Irf7* promoter in an RNA-independ-
497 ent, DNA-dependent fashion. SRSF7 is the only SR protein that encodes a Zn-knuckle, and to
498 date, this domain has been shown to enhance the RNA binding activity of SRSF7 (Cavaloc et
499 al., 1999; Cavaloc et al., 1994; Wang et al., 2021)). However, in other proteins, for example
500 TAF1, the largest subunit of the general transcription factor TFIIID, a Zn knuckle encourages

501 DNA binding and promoter occupancy (Curran et al., 2018). It is tempting to speculate that the
502 Zn finger domain in SRSF7 could promote its association directly with DNA. Future experiments
503 designed to implicate the Zn knuckle in SRSF7 association with the *Irf7* promoter and/or test the
504 ability of SRSF7 to directly bind DNA will help resolve the molecular mechanisms of SRSF7 pro-
505 moter enrichment.

506 In addition to linking SRSF7 to *Irf7* expression, our studies revealed an unexpected role
507 for SRSF7 in controlling tonic type I IFN expression in resting RAW cells (**Fig. 2A, E**) and MEFs
508 (**Fig. 2M-P**, time 0). These observations challenge the paradigm that IRF7 needs to be dramati-
509 cally upregulated before it can contribute to type I IFN responses. Indeed, differences in ISG ex-
510 pression were more robust in IRF7 KO RAW MΦs at rest than after LPS stimulation (**Fig. S4B)**.
511 These findings suggest that IRF7 is in fact the major mediator of the type I IFN response in rest-
512 ing macrophages, but *both* IRF3 and IRF7 contribute once they are activated downstream of
513 pattern recognition receptor engagement. To date, the role for IRF7 in maintaining tonic type I
514 IFN signaling has not been fully explored. Our RNA-seq data identify a specific regulon of ISGs
515 that is particularly sensitive to loss of IRF7 at baseline (**Fig. S3F, G**). Among the most downreg-
516 ulated genes in resting *Irf7* KO macrophages are several encoding guanylate binding proteins
517 (GBPs) and members of the oligoadenylate synthetase (OAS) family. Regulated expression of
518 these factors at baseline may reflect their role in directly mediating anti-viral and anti-bacterial
519 killing, with low level expression of these ISGs in resting cells providing an early advantage
520 upon infection. By demonstrating a role for IRF7 in maintaining tonic levels of these and other
521 ISGs, our results hint at additional roles for IRF7 in cellular homeostasis and disease that have
522 not been appreciated to date.

523 Consistent with this idea, growing evidence suggests that IRF7 expression in immune
524 cells is subject to multiple levels of control mediated by RBPs. Both mouse and human IRF7
525 genes encode very small introns (<100nt), an unusual adaptation in mammalian genomes. Reg-
526 ulated *IRF7* intron retention has been reported in THP-1 cells, wherein intron 2 is efficiently re-
527 moved upon monocyte-to-macrophage differentiation but not in resting monocytes (Green et al.,
528 2020). In response to treatment with TNF-α and IFN-α, as well as polyI:C transfection, regulated
529 removal of IRF7 intron 4 has been reported and was shown to be controlled by the RBP BUD13,
530 which is enriched on *Irf7* transcripts in BMDMs (Frankiw et al., 2019). Such regulation is pro-
531 posed to provide innate cells a way to limit the inappropriate expression of genes with high in-
532 flammatory potential like IRF7, while leaving cells poised to upregulate these genes when cer-
533 tain signals are received. We did not observe differences in the number of intron reads in *Srsf7*
534 KD vs. SCR RAW cells (**Fig. 3H**), nor did the MAJIQ algorithm identify SRSF7-dependent

535 alternative splicing changes in *Irf7* (**Fig. 1**). We propose that intron retention/alternative splicing
536 of *Irf7* by factors like BUD13 adds an additional layer of regulation on top of the transcriptional
537 control conferred by SRSF7. The fact that IRF7 is subject to regulation at multiple nodes argues
538 that it plays a larger than appreciated role in mediating inflammatory responses in immune cells.
539 Together, these previously published studies and our work presented here, argue that IRF7 is
540 required for basal maintenance and ramping up of type I interferon responses and highlights a
541 preeminent role for RNA binding proteins in regulating innate immune outcomes.
542

543 **ACKNOWLEDGEMENTS**

544 We would like the thank members of Patrick and Watson labs for critical reading of the
545 manuscript and invaluable feedback. We would also like to thank Phillip West and members of
546 his lab at Texas A&M School of Medicine for sharing reagents and protocols related to VSV in-
547 fection. Thanks to Susan Carpenter and her lab for sharing reagents and protocols related to
548 iBMDMs. and to the Genomic and RNA Profiling Core (GARP) at Baylor College of Medicine for
549 RNA-seq and ChIP-seq library generation and sequencing. Funding was provided by
550 NIH/NIGMS to KP (R35GM133720), NIH/NIAID to ROW and KP (R01AI155621), and
551 NIH/NIGMS to HMS (F31GM143893).
552

553 **DECLARATION OF INTERESTS**

554 The authors have no competing interests.

963 **Materials and Methods**

964

965 Cell culture

966 RAW 264.7 macrophage-like cells (RAW MΦs) (TIB-71™ ATCC) (originally isolated from male
967 BALB/c mice), L929 ISRE (Hoffpauir et al., 2020), *Irf7* KO RAW MΦs (this paper), and Lenti-X
968 cells (TaKaRa Bio) were cultured at 37 °C with a humidified atmosphere of 5% CO_2 in complete
969 media containing high glucose, DMEM (ThermoFisher) with 10% FBS (Millipore) 0.2% HEPES
970 (Thermo Fisher).

971

972 shRNA knockdowns

973 For RAW MΦs stably expressing scramble knockdown and *Srsf7* knockdown, Lenti-X cells were
974 transfected with a pSICO scramble non-targeting shRNA construct and pSICO *Srsf7* shRNA
975 constructs targeted at exon 3 and exon 4 of *Srsf7* using Polyjet (SignaGen Laboratories). Virus
976 was collected 24 and 48 h post transfection. RAW MΦs were transduced using Lipofectamine
977 2000 (Thermo Fischer). After 48 h, media was supplemented with Hygromycin (Invitrogen) to
978 select for cells containing the shRNA plasmid.

979

980 *S. enterica* (ser. Typhimurium)

981 *Salmonella enterica* serovar Typhimurium (SL1344) was obtained from Dr. Denise Monack,
982 Stanford. *S.* Typhimurium were streaked out on LB agar plates and incubated at 37°C overnight.

983

984 *S. enterica* (ser. Typhimurium) infections:

985 RAW MΦs were seeded in 12-well tissue culture-treated plates at a density of $7x10^5$ cells per cell,
986 and cultures of *S.* Typhimurium were grown at 37°C in LB broth containing 0.3M NaCl 16h prior
987 to infection. Bacterial cultures were diluted 1:20 3h prior to infection to reach mid-log phase OD_{600}
988 0.6-0.8. Mid-log phase bacteria were washed 3x with PBS and pelleted at 5,000 rpm for 3 min.
989 Bacteria were then added to DMEM (Hyclone) with 10% FBS (Sigma) and 2% HEPES (HyClone)
990 at an MOI of 5 for transcripts and MOI of 1 for replication. Infected cells were spun at 1,000 rpm
991 for 5 min then incubated for 10 min at 37 °C prior to gentamycin washes adding fresh media. At
992 indicated times post infection, cells were harvested with TRIzol for RNA isolation described below.

993

994 *M. tuberculosis*

995 The Erdman strain was used for all *M. tuberculosis* (Mtb) infections as well as Mtb luxBCADE a
996 luciferase expressing strain. Low passage lab stocks were thawed for each experiment to

997 ensure virulence was preserved. Mtb was cultured in roller bottles at 37 °C in Middlebrook 7H9
998 broth (BD Biosciences) supplemented with 10% OADC (BD Biosciences), 0.5% glycerol
999 (Fisher), and 0.1% Tween-80 (Fisher). All work with Mtb was performed under Biosafety Level 3
1000 containment using procedures approved by the Texas A&M University Institutional Biosafety
1001 Committee.
1002
1003 *Mtb in vitro* infections
1004 To prepare the inoculum, bacteria were grown to mid log phase (OD 0.6–0.8), spun at low
1005 speed (500 rcf) to remove clumps, and then pelleted and washed with PBS 2X. Resuspended
1006 bacteria were sonicated and spun at low speed again to further remove clumps. Then Mtb was
1007 then diluted in DMEM plus 10% horse serum (Gibco) and added to cells at a multiplicity of infec-
1008 tion (MOI) of 10 for RNA and protein analysis, a MOI of 5 for cell death studies, and a MOI of 1
1009 for bacterial growth assays. The day before the infection, RAW MΦs were plated on 12-well tis-
1010 sue culture–treated plates at a density of 3×10^5 cells per well or plated in corning 96 well black
1011 plates at $2.5\text{x}10^4$ cells/well and allowed to rest overnight. Cells were spun with bacteria for 10
1012 min at 1,000 rcf to synchronize infection, washed 2X with PBS, and then incubated in fresh me-
1013 dia. Where applicable, RNA was harvested from infected cells using 0.25 ml TRIzol reagent at
1014 each time point. For bacterial growth assays, RAW MΦs were plated on 12-well tissue culture–
1015 treated plates at a density of 2.5×10^5 cells per well. Luminescence was read for *M. tuberculosis*
1016 *luxBCADE* by lysing in 250 µl 0.5% Triton X-100 and dividing sample into duplicate wells of a
1017 96-well white bottomed plate (Costar). Luminescence was measured and normalized to back-
1018 ground using the luminescence feature of the INFINITE 200 PRO (Tecan) at 0, 48, 72 and 92 h
1019 post infection.
1020
1021 Vesicular stomatitis virus
1022 Recombinant *Vesicular stomatitis* virus (VSV; Indiana serotype) containing a GFP reporter
1023 cloned downstream of the VSV G-glycoprotein (VSV-G/GFP) was obtained collaboratively from
1024 Dr. John Rose at Yale School of Medicine though Dr. A. Phillip West at Texas A&M Health Sci-
1025 ence Center.
1026
1027 Vesicular stomatitis Virus (VSV) infections
1028 RAW MΦs were seeded in 12-well tissue culture-treated plates at a density of $7\text{x}10^5$ cells per
1029 well 16h before infection. The next day cells were infected with VSV-GFP virus (Dalton and
1030 Rose, 2001) at an MOI of 0.1 in serum-free DMEM (HyClone). After 1h of incubation with media

1031 containing virus, supernatant was removed, and fresh DMEM plus 10% FBS (Millipore) was
1032 added to each well. At indicated times post infection, cells were harvested with TRIzol for RNA
1033 isolation described below.
1034
1035 *M. musculus*
1036 Mice used in this study were C57BL6/J (Stock #00064) initially purchased from Jackson Labra-
1037 tory and afterward maintained with filial breeding. All mice used in experiments were compared
1038 to age- and sex- matched controls. Littermates were used for experiments. Mice used to gener-
1039 ate BMDMs were males between 10-16 weeks old. Embryos used to make primary MEFs were
1040 14.5 days post-coitum. All animals were housed, bred, and studied at Texas A&M Health Sci-
1041 ence Center under approved Institutional Care and Use Committee guidelines. All experiments
1042 for this study were reviewed and approved by the Texas A&M University Institutional Animal
1043 Care and Use Committee (AUP# 2019–0083). Mice were fed 4% standard chow and were kept
1044 on a 12 h light/dark cycle and provided food and water *ad libitum*. Mice were group housed
1045 (maximum 5 per cage) by sex on ventilated racks in temperature-controlled rooms.
1046
1047 Primary cell culture
1048 Bone marrow derived macrophages (BMDMs) were differentiated from bone marrow (BM) cells
1049 isolated by washing mouse femurs with 10 ml DMEM 1 mM sodium pyruvate. Cells were then
1050 centrifuged for 5 min at 400 rcf and resuspended in BMDM media (DMEM, 20% FBS (Millipore),
1051 1 mM sodium pyruvate (Lonza), 10% MCSF conditioned media (Watson lab)). BM cells were
1052 counted and plated at $5x10^6$ cells per 15 cm non-tissue culture treated dishes in 30 ml complete
1053 BMDM media. Cells were fed with an additional 15 ml of BMDM media on day 3. Cells were har-
1054 vested on day 7 with 1X PBS EDTA (Lonza).
1055
1056 Mouse embryonic fibroblasts (MEFs) were isolated from embryos. Briefly, embryos were dis-
1057 sected from yolk sacs, washed two times with cold 1X PBS, decapitated, and stripped of perito-
1058 neal contents. Headless embryos were disaggregated in cold 0.05% trypsin-EDTA (Lonza) and
1059 incubated on ice for 20 min., followed by incubation at 37 °C for an additional 20 min. Cells were
1060 then DNase treated with 4 ml disaggregation media (DMEM, 10% FBS, 100 µg/ml DNASE I
1061 (Worthington)) for 20 min at 37 °C. Isolated supernatants were spun down at 1000 rpm for 5
1062 min. Cells were resuspended in complete MEF media (DMEM, 10% FBS, 1 mM sodium py-
1063 ruvate), and plated in 15 cm tissue culture-treated dishes 1 dish per embryo in 25 ml of media.
1064 MEFs were allowed to expand for 2-3 days before harvest with 0.05% trypsin-EDTA (Lonza).

1065 iBMDMs were immortalized with J2 virus to generate iBMDMs.
1066
1067 siRNA knockdowns in MEFs
1068 Knockdown of mRNA transcripts was performed by plating $3x10^6$ MEFs in 10 cm plates and
1069 rested overnight. The following day complete media was replaced with 5 ml fresh complete me-
1070 dia 30 min prior to transfection. Cells were transfected using Fugene SI reagent 10 μM of siRNA
1071 stock against either *Srsf7* (ThermoFisher, s105011) or negative control, Silencer® Select Nega-
1072 tive Control #1 (4390843). Cells were incubated for 48h in transfection media at 37 °C with 5%
1073 CO_2 prior to downstream experiments.
1074
1075 siRNA knockdowns in BMDMs
1076 The day prior to transfection, $6x10^5$ BMDMs were seeded into 12-well plates. The day of trans-
1077 fection, 30nM of siRNA against *Srsf7* (ThermoFisher, s105011), against *Kmt5a/Setd8* (Ther-
1078 moFisher, s85986) or negative control, Silencer® Select Negative Control #1 (4390843) were
1079 mixed with 3 μl of LipoRNAiMAX (13778150, Thermo Fisher Scientific), incubated for 10m at
1080 room temperature, and then added into wells with 500 μl plain DMEM. Transfection proceeded
1081 for 6h and then wells were replenished with complete media.
1082
1083 Tetracycline inducible cell line generation
1084 For generation of tetracycline inducible RAW MΦs, pLenti CMV rtTA3 Blast (Addgene w756-1)
1085 stably expressing clonal RAW MΦs were transduced with pLenti CMV Puro DEST (Addgene
1086 w118-1) constructs containing 3xFL-GFP, 3xFL-SRSF7, and al 3xFL-SRSF7 phosphorylation
1087 mutants. After 48h, construct containing cells were selected through addition of puromycin (Invi-
1088 vogen). 1 μg/ml doxycycline (Sigma-Aldrich) treatment was used to activate construct expres-
1089 sion.
1090
1091 Cell stimulation for immune activation
1092 $7.5x10^5$ RAW MΦs were plated on 12-well tissue-culture treated plates 16h before cellular stim-
1093 ulation assays. The next day, cells were treated with lipopolysaccharide (LPS) from *E. coli* (Invi-
1094 vogen) at 100 ng/ml, or ISD (IDT, annealed in house) at 1 μg/ml, or IFN-β (PBL Assay Science)
1095 at 200 I/U per ml for the respective time points. Cells were collected for RNA isolation using Tri-
1096 zol reagent.
1097
1098 *Srsf7* KD mRNA sequencing and analysis

1099 As reported in Wagner, Scott and West et al. 2021, RNA-seq analysis was performed on RAW
1100 MΦs containing shRNA knockdowns of *Srsf6*, *Srsf2*, *Srsf1*, *Srsf7*, and *Srsf9* compared to SCR
1101 control with biological triplicates of each cell line. RNA-Seq and library preparation was per-
1102 formed by Texas A&M AgriLife Genomics and Bioinformatics Service. RNA samples were se-
1103 quenced on Illumina 4000 using 2 x 150-bp paired-end reads. Raw reads were filtered and
1104 trimmed and Fastq data was mapped to the Mus musculus Reference genome (RefSeq) using
1105 CLC Genomics Workbench 8.0.1. Differential expression analyses were performed using CLC
1106 Genomics Workbench. Relative transcript expression was calculated by counting Reads Per
1107 Kilobase of exon model per Million mapped reads (RPKM). Statistical significance was deter-
1108 mined by the EDGE test via CLC Genomics Workbench. Differentially expressed genes (DEGs)
1109 were selected as those with p value threshold < 0.05. Critical pathways affected by SR protein
1110 knockdown compared to control RAW MΦs, were analyzed by canonical pathway analysis using
1111 Ingenuity Pathway Analysis software from QIAGEN Bioinformatics. Genes that were differen-
1112 tially expressed with a p-value < 0.05 from our RNA-SEQ analysis were used as input. Inte-
1113 grated genomics viewer (IGV) visualization tracks were generated using the RNA-SEQ filtered
1114 and trimmed reads.
1115
1116 *Irf7* KO mRNA sequencing and analysis
1117 RNA- seq analysis was performed on control GFP KO or *Irf7* KO1 RAW MΦs in biological tripli-
1118 cate of each cell line. Data was analyzed by ROSALIND® (https://rosalind.bio/), with a
1119 HyperScale architecture developed by ROSALIND, Inc. (San Diego, CA). Reads were trimmed
1120 using cutadapt. Quality scores were assessed using FastQC. Reads were aligned to the Mus
1121 musculus genome build GRCm39 using STAR[3]. Individual sample reads were quantified using
1122 HTseq[4] and normalized via Relative Log Expression (RLE) using DESeq2 R library. Read Distri-
1123 bution percentages, violin plots, identity heatmaps, and sample MDS plots were generated as
1124 part of the QC step using RSeQC. DEseq2 was also used to calculate fold changes and p-val-
1125 ues and perform optional covariate correction. Clustering of genes for the final heatmap of dif-
1126 ferentially expressed genes was done using the PAM (Partitioning Around Medoids) method us-
1127 ing the fpc R library. Hypergeometric distribution was used to analyze the enrichment of path-
1128 ways, gene ontology, domain structure, and other ontologies. The topGO R library was used to
1129 determine local similarities and dependencies between GO terms in order to perform Elim prun-
1130 ing correction.
1131
1132 Alternative splicing analysis

1133 Modeling Alternative Junction Inclusion Quantification (MAJIQ) and the Voila visualization pack-
1134 age were used to model alternative splicing events with default parameters described by
1135 Vaquero-Garcia et al., 2016. Junction-spanning reads were used to construct splice graphs for
1136 transcripts by using the RefSeq annotation supplemented with de-novo (junctions not in the Ref-
1137 Seq transcriptome database but had sufficient evidence in the RNAseq data) detected junctions.
1138 Resulting splice graphs were analyzed for all identified local splice variations (LSVs). MAJIQ
1139 then quantified expected percent spliced in (PSI) value in control and knockdown samples for
1140 every junction in each LSV. Resulted viewed on VOILA were filtered for highest confidence
1141 change in LSVs (one or more junctions had at least a 95% probability of expected dPSI of at
1142 least an absolute value of 0.2 PSI units between control and knockdown.
1143
1144 RNA isolation and qPCR analysis
1145 For transcript analysis, cells and tissue were harvested in TRIzol and RNA was isolated using
1146 Direct-zol RNA Miniprep kits (Zymo Research) with 1 h DNase treatment. cDNA was synthe-
1147 sized with iScript cDNA Synthesis Kit (Bio-Rad). CDNA was diluted as appropriate for treatment,
1148 and a pool of cDNA was used to make a 1:3 standard curve with each standard sample diluted
1149 1:5 to produce a linear curve. RT-qPCR was performed using Power-Up SYBR Green Master
1150 Mix (Thermo Fisher) using a Quant Studio Flex6 (Applied Biosystems). Samples were run in
1151 triplicate wells in a 384-well plate. Averages of the raw values were normalized to average val-
1152 ues for the same sample with the control gene, *Actb*.
1153
1154 Semiquantitative qPCR analysis
1155 cDNA was synthesized by iScript cDNA Synthesis Kit (Bio-Rad) using an extended 1h amplifica-
1156 tion. Q5 high fidelity 2X Master mix (New England Biolabs) was used for PCR amplification us-
1157 ing targeted primers. Loading dye was added to PCR products and samples were run on 2%
1158 agarose gel containing ethidium bromide at 100 volts for 1 h. Gels were imaged on LiCOR Od-
1159 yssey Fc Dual-Mode Imaging System and bands were quantified.
1160
1161 Chromatin immunoprepitation
1162 $6x10^6$ RAW MΦs or BMDMs were seeded in a 10 cm dish, and 16h later stimulated for the indi-
1163 cated time. After stimulation cells were scraped, transferred to a 50 ml conical and fixed with 1%
1164 (v/v) formaldehyde for 10 min with gentle shaking. Formaldehyde was quenched with 0.125 M
1165 glycine for 5 min. Cells were pelleted and washed 1x with PBS, and then cells were lysed in 1
1166 ml of ChIP lysis buffer (150 mM NaCl, 5 mM EDTA, 0.5% NP-40 and 1% Triton X-100, 50 mM

1167 Tris-HCl, and protease/phosphatase inhibitor (added immediately before lysis) pH 7.5). Lysates
1168 were flash frozen, or ChIP proceeded by sonicating with for 40 min (30 sec on/off 10 min cycles)
1169 in a Bioruptor UCD-200 (Diagenode). Lysates were cleared and 10% taken for input samples.
1170 For RNA polymerase II, Y701 STAT1, IgG (isotype control) or H4K20me1 samples: 2 µg
1171 of the anti-pol II (Active Motif) or 2 µg of isotype control (IgG, Cell Signaling), 5ul Y701 STAT1
1172 (Cell Signaling), or 2 µg H4K20me1 (Invitrogen) (were incubated overnight at 4 with rotation.
1173 The following day, Pierce beads (Invitrogen) were washed 3x in ChIP buffer, blocked for 30 min
1174 with 100 µg salmon sperm DNA (Invitrogen) and 0.5 mg BSA, and washed once more with ChIP
1175 lysis buffer. Blocked beads were incubated with cleared chromatin immunocomplexes for 1h at
1176 4 °C with rotation. Beads were washed five times with ChIP buffer and then eluted with 250 µl of
1177 elution buffer (1% SDS and 0.1 M $NaHCO_3$) at 65 °C for 15 mins. The eluate and input were
1178 centrifuged and reverse the cross-links by adding 0.4 M NaCl for overnight at 55 °C. The next
1179 day, 1 µl of RNASE A (10 mg/ml, ThermoFisher) and 2 µl proteinase K (20 mg/ml, Ther-
1180 moFisher) were added to the samples and incubated for 1h at 55 °C while shaking. Samples
1181 were then subjected to Genomic Clean up and Concentrator (Zymo) to extract DNA. Purified in-
1182 put and IP DNA were analyzed by qRT-PCR using primers specific for the promoter region of
1183 target genes. Results were normalized to input. Data is presented as fold enrichment relative to
1184 intergenic control. Flag ChIP**:** As above except cleared lysates were added to blocked (as
1185 above) M2 anti-3xFLAG beads and protocol proceeded as above.
1186
1187 3x-FLAG ChIP-seq
1188 Data was analyzed by ROSALIND® (https://rosalind.bio/), with a HyperScale architecture devel-
1189 oped by ROSALIND, Inc. (San Diego, CA). Reads were trimmed using cutadapt[1]. Quality scores
1190 were assessed using FastQC[2]. Reads were aligned to the Mus musculus genome build mm10
1191 using bowtie2[3]. Per-sample quality assessment plots were generated with HOMER[4] and Mosa-
1192 ics[5]. Peaks were called using MACS2[6] (with input/IgG controls background subtracted, if pro-
1193 vided). Peak overlaps and differential binding were calculated using the DiffBind R library[7]. Dif-
1194 ferential binding was calculated at gene promoter sites. Read distribution percentages, identity
1195 heatmaps, and FRiP plots were generated as part of the QC step using ChIPQC R library[8] and
1196 HOMER. HOMER was also used to generate known and de novo motifs and perform functional
1197 enrichment analysis of pathways, gene ontology, domain structure and other ontologies.
1198
1199 CRISPR/Cas9 KO of *Irf7*

1200 Guide RNAs were generated to target the 3rd exon of *Irf7* using the Broad online tool
1201 (https://portals.broadinstitute.org/gppx/crispick/public) and synthesized by IDT. Primers were
1202 cloned into digested vector by phosphorylating, annealing, and ligating primers into LentiGuide-
1203 Puro (Addgene, plasmid 52963). Colonies were validated by Sanger sequencing using
1204 pLK0.1/hU6 promoter primer (Eton Biosciences, San Diego, CA). Lentivirus with sgRNAs were
1205 produced and used to transduce RAW MΦs stably expressing FL-Cas9 (Addgene, plasmid
1206 52962). After selection with 5 µg/ml puromycin knockout efficiency was analyzed by immunoblot
1207 and then sequencing for mutants by amplifying a 300 bp region of genomic DNA around exon 3.
1208 These PCR fragments were sequenced (as above) and compared to controls using TIDE analy-
1209 sis. The two best, most efficient sgRNA populations were clonally selected, expanded, and as-
1210 sayed for clones with total KO of IRF7 by immunoblot.
1211
1212 Protein quantification by immunoblot
1213 Cells were washed with PBS and lysed in 1X RIPA buffer with protease and phosphatase EDTA
1214 free inhibitors (Thermo Scientific), with the addition of 1 U/ml Benzonase (Millipore) to degrade
1215 genomic DNA. Proteins were separated by SDS-PAGE on Any kD mini-PROTEAN TGX precast
1216 gel (Bio-Rad) and transferred to 0.45µm nitrocellulose membranes (GE Healthcare). Mem-
1217 branes were blocked for 1h at RT in TBS +5% BSA. Blots were incubated overnight at 4 °C with
1218 the following primary antibodies: β-ACTIN (Abcam, 1:5000), Y701 STAT1 (Cell Signaling,
1219 1:1000), STAT1 (Cell Signaling, 1:1000), IRF7 (Cell Signaling, 1:1000), SRSF7 (Bethyl 1:3000)
1220 ZBP1 (Santa Cruz Biotechnologies, 1:1000), p-IRF3(S396) (Cell Signaling, 1:1000); IRF3
1221 (Bethyl, 1:1000); ANTI-FLAG M2 (Sigma Aldrich, 1:5000); Membranes were washed 3 x 5 min
1222 in PBS-Tween20 and incubated with appropriate secondary antibodies (LI-COR) for 1h at RT
1223 prior to imaging on a LiCOR Odyssey Fc Dual-Mode Imaging System.
1224
1225 Quantitation and Statistical Analysis
1226 Statistical analysis of data was performed using GraphPad Prism software. Two-tailed unpaired
1227 Student's t tests were used for statistical analyses, and unless otherwise noted, all results are
1228 representative of at least three biological samples (mean +/- SEM (n = 3 per group)).
1229
1230
1231

1232 **REFERENCES**

1233 Banks, D.A., Ahlbrand, S.E., Hughitt, V.K., Shah, S., Mayer-Barber, K.D., Vogel, S.N., El-Sayed,
1234 N.M., and Briken, V. (2019). Mycobacterium tuberculosis Inhibits Autocrine Type I IFN Signaling
1235 to Increase Intracellular Survival. J Immunol *202*, 2348-2359.
1236 Barrat, F.J., Crow, M.K., and Ivashkiv, L.B. (2019). Interferon target-gene expression and
1237 epigenomic signatures in health and disease. Nat Immunol *20*, 1574-1583.
1238 Barski, A., Cuddapah, S., Cui, K., Roh, T.Y., Schones, D.E., Wang, Z., Wei, G., Chepelev, I.,
1239 and Zhao, K. (2007). High-resolution profiling of histone methylations in the human genome.
1240 Cell *129*, 823-837.
1241 Bell, S.L., Lopez, K.L., Cox, J.S., Patrick, K.L., and Watson, R.O. (2021). Galectin-8 Senses
1242 Phagosomal Damage and Recruits Selective Autophagy Adapter TAX1BP1 To Control
1243 Mycobacterium tuberculosis Infection in Macrophages. mBio *12*, e0187120.
1244 Boguslawska, J., Sokol, E., Rybicka, B., Czubaty, A., Rodzik, K., and Piekielko-Witkowska, A.
1245 (2016). microRNAs target SRSF7 splicing factor to modulate the expression of osteopontin
1246 splice variants in renal cancer cells. Gene *595*, 142-149.
1247 Budzik, J.M., Swaney, D.L., Jimenez-Morales, D., Johnson, J.R., Garelis, N.E., Repasy, T.,
1248 Roberts, A.W., Popov, L.M., Parry, T.J., Pratt, D.*, et al.* (2020). Dynamic post-translational
1249 modification profiling of Mycobacterium tuberculosis-infected primary macrophages. Elife *9*.
1250 Caamano, J., and Hunter, C.A. (2002). NF-kappaB family of transcription factors: central
1251 regulators of innate and adaptive immune functions. Clin Microbiol Rev *15*, 414-429.
1252 Cavaloc, Y., Bourgeois, C.F., Kister, L., and Stevenin, J. (1999). The splicing factors 9G8 and
1253 SRp20 transactivate splicing through different and specific enhancers. RNA *5*, 468-483.
1254 Cavaloc, Y., Popielarz, M., Fuchs, J.P., Gattoni, R., and Stevenin, J. (1994). Characterization
1255 and cloning of the human splicing factor 9G8: a novel 35 kDa factor of the serine/arginine
1256 protein family. EMBO J *13*, 2639-2649.
1257 Cun, Y., An, S., Zheng, H., Lan, J., Chen, W., Luo, W., Yao, C., Li, X., Huang, X., Sun, X.*, et al.*
1258 (2021). Specific Regulation of m(6)A by SRSF7 Promotes the Progression of Glioblastoma.
1259 Genomics Proteomics Bioinformatics.
1260 Curran, E.C., Wang, H., Hinds, T.R., Zheng, N., and Wang, E.H. (2018). Zinc knuckle of TAF1 is
1261 a DNA binding module critical for TFIID promoter occupancy. Sci Rep *8*, 4630.
1262 de la Mata, M., and Kornblihtt, A.R. (2006). RNA polymerase II C-terminal domain mediates
1263 regulation of alternative splicing by SRp20. Nat Struct Mol Biol *13*, 973-980.

1264 Fitzgerald, K.A., Rowe, D.C., Barnes, B.J., Caffrey, D.R., Visintin, A., Latz, E., Monks, B., Pitha,
1265 P.M., and Golenbock, D.T. (2003). LPS-TLR4 signaling to IRF-3/7 and NF-kappaB involves the
1266 toll adapters TRAM and TRIF. J Exp Med *198*, 1043-1055.
1267 Frankiw, L., Majumdar, D., Burns, C., Vlach, L., Moradian, A., Sweredoski, M.J., and Baltimore,
1268 D. (2019). BUD13 Promotes a Type I Interferon Response by Countering Intron Retention in
1269 Irf7. Mol Cell *73*, 803-814 e806.
1270 Fu, Y., and Wang, Y. (2018). SRSF7 knockdown promotes apoptosis of colon and lung cancer
1271 cells. Oncol Lett *15*, 5545-5552.
1272 Gao, D., Ciancanelli, M.J., Zhang, P., Harschnitz, O., Bondet, V., Hasek, M., Chen, J., Mu, X.,
1273 Itan, Y., Cobat, A.*, et al.* (2021). TLR3 controls constitutive IFN-beta antiviral immunity in human
1274 fibroblasts and cortical neurons. J Clin Invest *131*.
1275 Gough, D.J., Messina, N.L., Clarke, C.J., Johnstone, R.W., and Levy, D.E. (2012). Constitutive
1276 type I interferon modulates homeostatic balance through tonic signaling. Immunity *36*, 166-174.
1277 Green, I.D., Pinello, N., Song, R., Lee, Q., Halstead, J.M., Kwok, C.T., Wong, A.C.H., Nair, S.S.,
1278 Clark, S.J., Roediger, B.*, et al.* (2020). Macrophage development and activation involve
1279 coordinated intron retention in key inflammatory regulators. Nucleic Acids Res *48*, 6513-6529.
1280 Gu, J., Shi, J., Wu, S., Jin, N., Qian, W., Zhou, J., Iqbal, I.G., Iqbal, K., Gong, C.X., and Liu, F.
1281 (2012). Cyclic AMP-dependent protein kinase regulates 9G8-mediated alternative splicing of tau
1282 exon 10. FEBS Lett *586*, 2239-2244.
1283 Gu, L., Casserly, D., Brady, G., Carpenter, S., Bracken, A.P., Fitzgerald, K.A., Unterholzner, L.,
1284 and Bowie, A.G. (2022). Myeloid cell nuclear differentiation antigen controls the pathogen-
1285 stimulated type I interferon cascade in human monocytes by transcriptional regulation of IRF7.
1286 Nat Commun *13*, 14.
1287 Hoffpauir, C.T., Bell, S.L., West, K.O., Jing, T., Wagner, A.R., Torres-Odio, S., Cox, J.S., West,
1288 A.P., Li, P., Patrick, K.L.*, et al.* (2020). TRIM14 Is a Key Regulator of the Type I IFN Response
1289 during Mycobacterium tuberculosis Infection. J Immunol *205*, 153-167.
1290 Honda, K., and Taniguchi, T. (2006). IRFs: master regulators of signalling by Toll-like receptors
1291 and cytosolic pattern-recognition receptors. Nat Rev Immunol *6*, 644-658.
1292 Honda, K., Yanai, H., Negishi, H., Asagiri, M., Sato, M., Mizutani, T., Shimada, N., Ohba, Y.,
1293 Takaoka, A., Yoshida, N.*, et al.* (2005). IRF-7 is the master regulator of type-I interferon-
1294 dependent immune responses. Nature *434*, 772-777.
1295 Huang, R., Grishagin, I., Wang, Y., Zhao, T., Greene, J., Obenauer, J.C., Ngan, D., Nguyen,
1296 D.T., Guha, R., Jadhav, A.*, et al.* (2019). The NCATS BioPlanet - An Integrated Platform for

1297 Exploring the Universe of Cellular Signaling Pathways for Toxicology, Systems Biology, and
1298 Chemical Genomics. Front Pharmacol *10*, 445.
1299 Jefferies, C.A. (2019). Regulating IRFs in IFN Driven Disease. Front Immunol *10*, 325.
1300 Jeong, S. (2017). SR Proteins: Binders, Regulators, and Connectors of RNA. Mol Cells *40*, 1-9.
1301 Ji, X., Zhou, Y., Pandit, S., Huang, J., Li, H., Lin, C.Y., Xiao, R., Burge, C.B., and Fu, X.D.
1302 (2013). SR proteins collaborate with 7SK and promoter-associated nascent RNA to release
1303 paused polymerase. Cell *153*, 855-868.
1304 Kadota, Y., Jam, F.A., Yukiue, H., Terakado, I., Morimune, T., Tano, A., Tanaka, Y., Akahane,
1305 S., Fukumura, M., Tooyama, I.*, et al.* (2020). Srsf7 Establishes the Juvenile Transcriptome
1306 through Age-Dependent Alternative Splicing in Mice. iScience *23*, 100929.
1307 Kajigaya, H., Ishibashi, T., Hayashi, A., Yamaguchi, Y., and Baba, H. (2016). Concentration of
1308 neddylation-related molecules in paranodal myelin of the peripheral nervous system. Proc Jpn
1309 Acad Ser B Phys Biol Sci *92*, 56-68.
1310 Katsuyama, T., and Moulton, V.R. (2021). Splicing factor SRSF1 is indispensable for regulatory
1311 T cell homeostasis and function. Cell Rep *36*, 109339.
1312 Konigs, V., de Oliveira Freitas Machado, C., Arnold, B., Blumel, N., Solovyeva, A., Lobbert, S.,
1313 Schafranek, M., Ruiz De Los Mozos, I., Wittig, I., McNicoll, F.*, et al.* (2020). SRSF7 maintains its
1314 homeostasis through the expression of Split-ORFs and nuclear body assembly. Nat Struct Mol
1315 Biol *27*, 260-273.
1316 Lemaire, R., Winne, A., Sarkissian, M., and Lafyatis, R. (1999). SF2 and SRp55 regulation of
1317 CD45 exon 4 skipping during T cell activation. Eur J Immunol *29*, 823-837.
1318 Loomis, R.J., Naoe, Y., Parker, J.B., Savic, V., Bozovsky, M.R., Macfarlan, T., Manley, J.L., and
1319 Chakravarti, D. (2009). Chromatin binding of SRp20 and ASF/SF2 and dissociation from mitotic
1320 chromosomes is modulated by histone H3 serine 10 phosphorylation. Mol Cell *33*, 450-461.
1321 Luco, R.F., Allo, M., Schor, I.E., Kornblihtt, A.R., and Misteli, T. (2011). Epigenetics in
1322 alternative pre-mRNA splicing. Cell *144*, 16-26.
1323 Luco, R.F., Pan, Q., Tominaga, K., Blencowe, B.J., Pereira-Smith, O.M., and Misteli, T. (2010).
1324 Regulation of alternative splicing by histone modifications. Science *327*, 996-1000.
1325 MacMicking, J.D., North, R.J., LaCourse, R., Mudgett, J.S., Shah, S.K., and Nathan, C.F.
1326 (1997). Identification of nitric oxide synthase as a protective locus against tuberculosis. Proc
1327 Natl Acad Sci U S A *94*, 5243-5248.
1328 MacMicking, J.D., Taylor, G.A., and McKinney, J.D. (2003). Immune control of tuberculosis by
1329 IFN-gamma-inducible LRG-47. Science *302*, 654-659.

1330 Misteli, T., Caceres, J.F., Clement, J.Q., Krainer, A.R., Wilkinson, M.F., and Spector, D.L.
1331 (1998). Serine phosphorylation of SR proteins is required for their recruitment to sites of
1332 transcription in vivo. J Cell Biol *143*, 297-307.
1333 Muller-McNicoll, M., Botti, V., de Jesus Domingues, A.M., Brandl, H., Schwich, O.D., Steiner,
1334 M.C., Curk, T., Poser, I., Zarnack, K., and Neugebauer, K.M. (2016). SR proteins are NXF1
1335 adaptors that link alternative RNA processing to mRNA export. Genes Dev *30*, 553-566.
1336 Nikolaou, K.C., Moulos, P., Harokopos, V., Chalepakis, G., and Talianidis, I. (2017). Kmt5a
1337 Controls Hepatic Metabolic Pathways by Facilitating RNA Pol II Release from Promoter-
1338 Proximal Regions. Cell Rep *20*, 909-922.
1339 Ning, S., Pagano, J.S., and Barber, G.N. (2011). IRF7: activation, regulation, modification and
1340 function. Genes Immun *12*, 399-414.
1341 Pandey, A., Ding, S.L., Qin, Q.M., Gupta, R., Gomez, G., Lin, F., Feng, X., Fachini da Costa, L.,
1342 Chaki, S.P., Katepalli, M.*, et al.* (2017). Global Reprogramming of Host Kinase Signaling in
1343 Response to Fungal Infection. Cell Host Microbe *21*, 637-649 e636.
1344 Schoggins, J.W. (2019). Interferon-Stimulated Genes: What Do They All Do? Annu Rev Virol *6*,
1345 567-584.
1346 Schoggins, J.W., and Rice, C.M. (2011). Interferon-stimulated genes and their antiviral effector
1347 functions. Curr Opin Virol *1*, 519-525.
1348 Schoggins, J.W., Wilson, S.J., Panis, M., Murphy, M.Y., Jones, C.T., Bieniasz, P., and Rice,
1349 C.M. (2011). A diverse range of gene products are effectors of the type I interferon antiviral
1350 response. Nature *472*, 481-485.
1351 Shin, C., Feng, Y., and Manley, J.L. (2004). Dephosphorylated SRp38 acts as a splicing
1352 repressor in response to heat shock. Nature *427*, 553-558.
1353 Sin, W.X., Yeong, J.P., Lim, T.J.F., Su, I.H., Connolly, J.E., and Chin, K.C. (2020). IRF-7
1354 Mediates Type I IFN Responses in Endotoxin-Challenged Mice. Front Immunol *11*, 640.
1355 Smale, S.T. (2012). Transcriptional regulation in the innate immune system. Curr Opin Immunol
1356 *24*, 51-57.
1357 Song, J., Su, Z.Z., and Shen, Q.M. (2020). Long non-coding RNA MALAT1 regulates
1358 proliferation, apoptosis, migration and invasion via miR-374b-5p/SRSF7 axis in non-small cell
1359 lung cancer. Eur Rev Med Pharmacol Sci *24*, 1853-1862.
1360 Tellier, M., Maudlin, I., and Murphy, S. (2020). Transcription and splicing: A two-way street.
1361 Wiley Interdiscip Rev RNA *11*, e1593.

1362 ten Dam, G.B., Zilch, C.F., Wallace, D., Wieringa, B., Beverley, P.C., Poels, L.G., and Screaton,
1363 G.R. (2000). Regulation of alternative splicing of CD45 by antagonistic effects of SR protein
1364 splicing factors. J Immunol *164*, 5287-5295.
1365 van Nuland, R., and Gozani, O. (2016). Histone H4 Lysine 20 (H4K20) Methylation, Expanding
1366 the Signaling Potential of the Proteome One Methyl Moiety at a Time. Mol Cell Proteomics *15*,
1367 755-764.
1368 Vaquero-Garcia, J., Barrera, A., Gazzara, M.R., Gonzalez-Vallinas, J., Lahens, N.F.,
1369 Hogenesch, J.B., Lynch, K.W., and Barash, Y. (2016). A new view of transcriptome complexity
1370 and regulation through the lens of local splicing variations. Elife *5*, e11752.
1371 Veloso, A., Kirkconnell, K.S., Magnuson, B., Biewen, B., Paulsen, M.T., Wilson, T.E., and
1372 Ljungman, M. (2014). Rate of elongation by RNA polymerase II is associated with specific gene
1373 features and epigenetic modifications. Genome Res *24*, 896-905.
1374 Wagner, A.R., Scott, H.M., West, K.O., Vail, K.J., Fitzsimons, T.C., Coleman, A.K., Carter, K.E.,
1375 Watson, R.O., and Patrick, K.L. (2021). Global Transcriptomics Uncovers Distinct Contributions
1376 From Splicing Regulatory Proteins to the Macrophage Innate Immune Response. Front Immunol
1377 *12*, 656885.
1378 Wagner, A.R., Weindel, C.G., West, K.O., Scott, H.M., Watson, R.O., and Patrick, K.L. (2022).
1379 SRSF6 balances mitochondrial-driven innate immune outcomes through alternative splicing of
1380 BAX. Elife *11*.
1381 Wagner, R.E., and Frye, M. (2021). Noncanonical functions of the serine-arginine-rich splicing
1382 factor (SR) family of proteins in development and disease. Bioessays *43*, e2000242.
1383 Wang, H.Y., Xu, X., Ding, J.H., Bermingham, J.R., Jr., and Fu, X.D. (2001). SC35 plays a role in
1384 T cell development and alternative splicing of CD45. Mol Cell *7*, 331-342.
1385 Wang, Y., Yu, Y., Pang, Y., Yu, H., Zhang, W., Zhao, X., and Yu, J. (2021). The distinct roles of
1386 zinc finger CCHC-type (ZCCHC) superfamily proteins in the regulation of RNA metabolism.
1387 RNA Biol *18*, 2107-2126.
1388 Watson, R.O., Bell, S.L., MacDuff, D.A., Kimmey, J.M., Diner, E.J., Olivas, J., Vance, R.E.,
1389 Stallings, C.L., Virgin, H.W., and Cox, J.S. (2015). The Cytosolic Sensor cGAS Detects
1390 Mycobacterium tuberculosis DNA to Induce Type I Interferons and Activate Autophagy. Cell
1391 Host Microbe *17*, 811-819.
1392 Xu, Q., Shi, J., Zhang, L., Sheng, Y., Zhang, Y., Chu, D., and Xu, A. (2022). Circ_0006006
1393 facilitates non-small cell lung cancer progression by modulating miR-924/SRSF7 axis. J Gene
1394 Med *24*, e3411.

1395 Zhong, X.Y., Ding, J.H., Adams, J.A., Ghosh, G., and Fu, X.D. (2009). Regulation of SR protein
1396 phosphorylation and alternative splicing by modulating kinetic interactions of SRPK1 with
1397 molecular chaperones. Genes Dev *23*, 482-495.
1398 Zhou, Z., and Fu, X.D. (2013). Regulation of splicing by SR proteins and SR protein-specific
1399 kinases. Chromosoma *122*, 191-207.
1400